into gibbons via the subcutaneous and vaginal route. Moreover, saliva of carrier patients was pooled and inoculated into gibbons via the subcutaneous and oral route. The results showed that semen and saliva from carrier patients cause asymptomatic disease in gibbons when transmitted via the subcutaneous or vaginal route, yet not via the oral route (Scott et al., 1980).

In addition to these experiments, Mimms et al. performed studies by infecting a chimpanzee with gibbon HBV. The HBV-DNA sequence from this chimpanzee was similar to that of gibbon HBV (Mimms et al., 1993). In conclusion, human HBV can be transmitted to non-human primates and cross-species transmission of non-human primate HBV can occur among various non-human primate species. However, cross-species transmission of non-human primate HBV to humans has not yet been supported by scientific evidence. To avoid performing experiments in humans, severe combined immunodeficiency mice transgenic for urokinase-type plasminogen activator, with the liver replaced with human hepatocytes (chimeric mice) serve as a suitable model for studies on human liver-specific pathogens such as HCV and HBV, human hepatic metabolism of pharmaceutical agents, and human hepatic toxicity of candidate anti-proliferative agents (Kneteman and Mercer, 2005). The mice present evidence that more fully characterizes the repopulation of the mouse liver with human hepatocytes (Meuleman et al., 2005). Histological studies have revealed that chimeric mice show evidence of human hepatocyte replace integration with infiltration into mouse liver. Moreover, human albumin and 21 other human specific proteins can be detected in mouse sera (Dandri et al., 2001; Mercer et al., 2001). Subsequently, these mice were used to support woodchuck and human hepatocyte culture and were supported infection with woodchuck hepatitis virus (WHV) and HBV (Meuleman et al., 2005; Petersen et al., 1998; Tabuchi et al., 2008).

The aim of this study has been to demonstrate that non-human primate HBV can be replicated in human hepatocytes in order to consider preventive measures in case of potential HBV transmission from non-human primates to humans.

2. Materials and methods

The study was approved by the Faculty of Veterinary Science, Animal Care and Use Committee, Mahidol University. All experiments were performed in a biosafety level 2 laboratory.

2.1. Gibbon and orangutan HBsAg-positive serum

To study cross-species transmission of non-human primate HBV to humans, the HBsAg and HBV-DNA positive sera of white-cheeked gibbon (*Nomascus leucogenys*) and orangutan (*P. pygmaeus*) were collected from Dusit zoo, Bangkok and Khao Pratub Chang Wildlife Breeding Center, Ratchaburi, Thailand, respectively. These sera constitute the stored surplus sera from a previous study (Sa-nguanmoo et al., 2008).

2.2. Chimeric mice inoculation

Twelve-week-old SCID mice transgenic for urokinase-type plasminogen activator with human hepatocytes (PhoenixBio Co, Ltd., Hiroshima, Japan) were used in this study (Tateno et al., 2004). Real-time PCR was employed to detect non-human primate HBV DNA concentration in gibbon and orangutan serum. This detection method has been shown elsewhere (Abe et al., 1999).

The minimum infectious dose of pre-acute and late acute HBV for HBV transmission to chimeric mice with human hepatocyte repopulation is approximately 10^0 and 10^2 copies (Tabuchi et al., 2008). In this study, 10^4 gibbon or orangutan HBV genome equivalents were intravenously inoculated into 3 chimeric mice of each group. However, none of the chimeric mice showed evidence of HBV markers until week 4 after inoculation. Then, all chimeric mice were re-inoculated with 10^5 genome equivalents.

2.3. Serum collection and HBV DNA extraction

Twenty microliter serum samples were collected once a week after inoculation. HBV DNA was extracted from 5 μl mouse sera by using the QIAamp® DNA Mini kit (QIAGEN, QIAGEN Sciences Inc., MD) following the manufacturer's recommendation.

2.4. HBV DNA quantitative method

HBV DNA quantity was determined by real-time PCR (ABI 7500 Fast Real-time PCR, Applied Biosystems, Foster City, CA). To that end, the small S region was amplified as previously described (Abe et al., 1999). Briefly, 5 μl of DNA were subjected to quantitative HBV DNA analysis by ABI 7500 Fast Real-time PCR (Applied Biosystems, Foster City, CA). The reaction mixture comprised 12.5 μl TaqMan® Universal PCR MasterMix (Applied Biosystems, Foster City, CA), 0.5 μl of 10 μM forward primer (HBSF2: 5′-CTTCATCCTGCTGCTATGCCT-3′), 0.5 μl of 10 μM reverse primer (HBSR2: 5′-AAAGCCCAGGATGATGGGAT-3′), 0.5 μl of 10 μM probe (HBSP2G: FAM-ATGTTGCC CGTTTGTCCTCTAATTCCAG-TAMRA) and 6 μl distilled water. The real-time PCR was performed under the following conditions: 95 °C for 10 min, followed by 45 cycles of 95 °C for 15 s and 60 °C for 30 s, and 4 °C for the holding step. The HBV viral load in unknown samples was calculated by comparison with the standard curve. The detection limit in this study was 1000 copies/ml due to the small sample volume.

2.5. DNA extraction from mouse liver tissue and cccDNA detection in liver and sera of infected chimeric SCID mice

Mouse liver tissues from one HBV-DNA positive mouse each from the gibbon and orangutan HBV inoculation group were collected at week 15 after inoculation. To extract DNA from mouse liver tissue, 25 mg of liver tissue were extracted by using the DNeasy® Blood & Tissue kit (QIAGEN, QIAGEN Sciences Inc., MD) and eluted in 200 μl of elution buffer. HBV cccDNA was detected by conventional PCR (GeneAmp® PCR System 9700, Applied Biosystems, Foster City, CA). Primer sequences have been previously published (Suzuki et al., 2009). Partially double-stranded HBV DNA could not be amplified by these primers. The details have been previously described (Mason et al., 1998). Briefly, 5 μl of DNA were subjected to amplification by GeneAmp® PCR System 9700 (Applied Biosystems, Foster City, CA). The reaction mixture comprised 1 U of Ampli Taq Gold® (Applied Biosystems, Foster City, CA), 2.5 μl of 10× PCR buffer containing 15 mM $MgCl_2$, 2 μl of GeneAmp® dNTP Mix (Applied Biosystems, Washington, UK), 1 μl of 10 μM forward primer (cccF2: 5′-CGTCTGTGCCTTCTCATCTGA-3′), 1 μl of 10 μM reverse primer (cccR4: 5′-GCACAGCTTGGAGGCTTGAA-3′), and 13.3 μl distilled water. The PCR was performed under the following conditions: 96 °C for 10 min, followed by 45 cycles of 95 °C for 30 s, 60 °C for 30 s, and 72 °C for 45 s, and 4 °C for the holding step.

2.6. Entire genome sequencing and phylogenetic analysis

Mouse serum samples positive for HBV DNA were subjected to further studies by sequencing the entire genome sequences. To amplify the entire genome, 1 μl of DNA re-suspended solution was used as template for round I PCR. The entire genome was distinguished into two segments (fragment A and fragment B). Fragment A was amplified by 10 μM forward primer (HBV17F-SARU: 5′-CAAACTCTGCAAGATCCCAGAG-3′) and 10 μM reverse

primer (HBV1799R-SARU 5′-GACCAATTTATGCCTACAGCCTC-3′). Fragment B was amplified by 10 μM forward primer (HBV1595F-SARU: 5′-CTTCACCTCTGCACGTTGCATGG-3′) and 10 μM reverse primer (HBV262R-SARU: 5′-CCACCACGAGTCTAGACTCTGTGG-3′). Both fragment A and fragment B used the same reaction mixture as follows: 5 μl of 2.5 mM dNTP, 2 μl of 10 μM forward primer, 2 μl of 10 μM forward primer, 0.33 μl of LA-Taq (TaKaRa BIO INC, Shiga, Japan), and 29.67 μl distilled water. The amplification method was performed on GeneAmp® PCR System 9700 (Applied Biosystems, Foster City, CA). The thermal cycle was continued as follows: 95 °C for 2 min (pre-denaturation) and followed by 35 cycles of 94 °C for 30 s, 60 °C for 30 s and 72 °C for 2 min, and 72 °C for 15 min (final extension).

For the second round PCR, 2 μl of round I PCR was used as template. Round I PCR product of fragment A was nested by HBV47F-SARU forward primer (5′-CTGTATTTTCCTGC-TGGTGGCTCCAG-3′) and HBV1760R-SARU reverse primer (5′-TAACCTCGTCTCCGCCCCAAACTC-3′). The first round I PCR product of fragment B was nested by HBV1608F-SARU forward primer (5′-GCATGGAGACCACCGTGAACG-3′) and HBV201R-SARU reverse primer (5′-TGTAACACGAGCAGGGGTCCTAGG-3′). Both fragment A and fragment B used reaction mixtures as round I PCR except increasing in the first round PCR template to 2 μl and adjusting distilled water to 28.67 μl. The amplification program was performed as follows: 95 °C for 2 min (pre-denaturation) and followed by 35 cycles of 94 °C for 30 s, 60 °C for 30 s and 72 °C for 2 min, and 72 °C for 20 min (final extension).

The second round PCR products were segregated by electrophoresis on 1% agarose gel stained with ethidium bromide. The bands of PCR products were purified using the QIAquick Gel Extraction kit (QIAGEN GmbH, Hilden, Germany). Purified products were further analyzed by ABI PRISM 3100 Genetic Analyzer (Applied Biosystems, Foster City, CA).

The genome was sequenced using the 8 primer sets previously published (Sugauchi et al., 2001). Cycle sequencing was performed using the BigDye Terminator 3.1V cycle sequencing kit (Applied Biosystems, Foster City, CA) according to the manufacturer's recommendations. The conditions for sequencing were programmed into the GeneAmp® PCR System 9700 (Applied Biosystems, Foster City, CA) as previously reported (Sugauchi et al., 2001). Nucleotide sequences were edited and assembled using SEQMAN 4.00 (LASERGENE program package, DNASTAR, DNASTAR Inc., Madison, WI). All complete HBV genomes isolated from mouse sera were compared to nucleotide sequences available at the GenBank database by using the Blast program (NCBI, Bethesda, MD). Moreover, the HBV sequences obtained from mouse sera were compared with gibbon and orangutan HBV strains determined prior to inoculation and also compared with other non-human primate HBVs and each human genotype from the GenBank database (NCBI, Bethesda, MD). Genetic comparison was performed by Clustal X program version 2.0.10 (European Bioinformatics Institute, Cambridge, UK). Subsequently, the phylogenetic tree was constructed using the Tamura – 3 parameter neighbor-joining method by Molecular Evolutionary Genetics Analysis (MEGA) software version 4.0 (The Biodesign Institute, Tempe, AZ).

2.7. HBsAg, HBcrAg, and human albumin measurement in mouse sera

Mouse sera were diluted (1:10) and subjected to chemiluminescence enzyme immunoassay (CLEIA) (Fujirebio Diagnostic, Inc., Tokyo, Japan) to detect HBV surface antigen (HBsAg) and HBV core – related antigen: – the antigen which includes both the HBV precore/core proteins (HBcrAg) (Kimura et al., 2005; Shinkai et al., 2006). HBcrAg measurement by this assay implies detection of precore/core proteins, including core protein and HBeAg (Kimura et al., 2002, 2005; Rokuhara et al., 2003; Wong et al., 2007). HBcrAg also showed a good correlation with HBV DNA levels in Asian patients (Kimura et al., 2002; Rokuhara et al., 2003, 2005) and intrahepatic parameters, including fibrosis scores, intrahepatic HBV, cccDNA and nuclear HBcAg (Wong et al., 2007). To expose the core protein and HBeAg, the diluted serum was fist incubated with the solution that contains sodium dodecylsulfate. Subsequently, the lysate was added to the plate coated with primary antibody to HBcAg and HBeAg. After incubation, the plate was washed to discard excess primary antibody and the second antibody labeled with alkaline phosphatase was added. Upon addition of substrate solution, the incubated reaction was measured by chemiluminescent enzyme immunoassay (CLEIA). Fully automated analysis was performed using the Lumipulse® System (Fujirebio Diagnostic, Inc., Tokyo, Japan). Human serum albumin (h-Alb) levels were determined applying a commercial enzyme linked immunosorbent (ELISA) test kit (Bethyl Laboratories Inc., Montgomery, TX).

2.8. Immunohistofluorescence assay

To detect HBcAg and human albumin, thick mouse liver tissue was prepared by cutting the frozen mouse liver with a Leica CM1900 Cryostat-microtome (Meyer Instruments, Inc., Houston, TX) and mounting the slices on glass slides. Histological analysis was performed by immunofluorescence assay as previously reported (Sugiyama et al., 2006). Briefly, mouse liver tissue was blocked by DakoCytomation antibody diluent (Dako North America, Inc., Carpinteria, CA) for 10 min at room temperature. After drying by air, the tissue was incubated in the dark with 50 μg/ml of polyclonal rabbit anti-hepatitis B virus core antigen (HBcAg) (Dako North America, Inc., Carpinteria, CA) for 1 h at 37 °C. After washing 5 times with 1× phosphate buffered saline (PBS) (GIBCO, Invitrogen Corporation, Carlsbad, CA) the tissue was incubated with 50 μg/ml of Cy3® goat anti-rabbit IgG (H+L) (Invitrogen Molecular Probes, Eugene, OR) or 5 μg/ml of goat anti-human albumin FITC (Bethyl Laboratories, Inc., Montgomery, TX) in the dark at 37 °C for 1 h. After washing 5 times with 1× PBS, the tissue was mounted by VECTASHIELD mounting medium with DAPI (Vector Laboratories, Inc., Birmingham, CA). The stained mouse tissue was examined under a Nikon Microscope ECLIPSE E800 (Nikon Instruments, Inc., Melville, NY).

3. Results

3.1. Serum HBV DNA, HBsAg, HBcrAg and human albumin level quantitation

Upon first inoculation with serum containing 10^4 copies of gibbon or orangutan HBV, none of the mice could be infected. Then, chimeric mice were re-inoculated with 10^5 copies. One mouse died before re-inoculation. After re-inoculation, mouse sera were collected once a week. Samples were subjected to quantitative HBV DNA analysis by real-time PCR while HBsAg and HBcrAg were quantitatively determined by CLIEA. Four of 5 mice could be infected with gibbon or orangutan HBV. Two mice each from the gibbon and orangutan groups showed levels of HBV DNA, HBsAg, and HBcrAg with the remaining mouse not displaying any of these markers. In detail, HBV DNA and HBcrAg could be detected in serum samples from two mice of the gibbon group (code 101 and 103) and two mice of the orangutan group (code 201 and 202) 4 weeks after inoculation. HBsAg was present in the orangutan group 4 weeks and in the gibbon groups 6 weeks after inoculation, respectively.

In this experiment, the expected HBV markers HBV DNA, HBsAg and HBcrAg could be detected in mouse serum around 4–5 weeks after inoculation. This finding matched previous studies that had

inoculated human HBV genotypes A2, C2, B1 and J into chimeric SCID mice (Sugiyama et al., 2009; Tatematsu et al., 2009). The time appearance and progression of non-human primate HBV markers presented as same as with human HBV markers (Ganem and Prince, 2004). Human albumin (h-Alb) was measured by ELISA as a quality control. Serum h-Alb levels prior to inoculation of all mice in this study exceeded 7 mg/ml indicating a human hepatocyte replacement index (RI) of over 70 percent (PhoenixBio Co, Ltd., Hiroshima, Japan) and were stable during the experiment (Fig. 1). Mean alanine aminotransferase (ALT) levels were around 200 IU/L in the uPA/SCID mouse sera. After non-human primate HBV inoculation, ALT levels slightly increased in this study (data not shown).

3.2. Intrahepatic cccDNA detection in liver tissue and mouse sera

Using the specific primers that amplify only cccDNA (Suzuki et al., 2009), HBV cccDNA was detected in mouse liver tissue from those mice that had been infected with gibbon and orangutan HBV (Fig. 2A). Moreover, cccDNA was found in the sera of mice infected with gibbon HBV (Fig. 2B).

3.3. Phylogenetic analysis of the entire HBV genome from mouse sera

HBV-DNA from all four mice was amplified and subjected to sequencing of the entire genome. The sequences from mouse sera were identical to HBV from gibbon or orangutan serum determined prior to inoculation (gibbon code GD14, GenBank ID: HQ603061; orangutan code OS25, GenBank ID: EU155824) (Fig. 3). Comparison between the complete HBV sequences from mouse sera and gibbon or orangutan sera prior to inoculation showed 99.9% and 100% similarity, respectively.

3.4. HBcAg and human albumin detection in mouse liver tissue

The mouse liver was also tested for HBcAg by staining with polyclonal rabbit anti-HBcAg and goat anti-rabbit IgG labeled with Cy3 (Fig. 4A). To locate the human hepatocyte area in chimeric mouse liver, the tissue was examined for human albumin. The same mouse liver tissue was stained with goat anti-human albumin conjugated with FITC (Fig. 4B). The study confirmed that HBcAg was found in the same area of human hepatocytes (Fig. 4C).

4. Discussion

In a previous study, Hu et al. (2000) constructed a phylogenetic tree and found that the *S* gene sequence from two chimpanzees clustered with human HBV genotypes A and C which could suggest possible virus transmission from human to chimpanzee. Currently, there is no evidence indicating natural infection of humans with non-human primate HBV (Noppornpanth et al., 2003). However, non-human primate HBV would be transmitted to humans because the respective HBV genomes are largely similar.

In this study, cross-species transmission was performed using chimeric mice containing human hepatocytes. The results showed that HBV-DNA, HBsAg and HBcrAg can be detected in sera of mice inoculated with HBV-DNA positive sera from orangutan or gibbon carriers. Detection of HBV cccDNA in liver as well as immune staining data have provided the evidence that gibbon and orangutan HBV can be replicated in human hepatocytes of the chimeric mice sero-positive for HBV DNA. HBsAg and HBV DNA concentrations could increase over time following inoculation. Interestingly, based on phylogenetic analysis, all strains of HBV sequences obtained from mouse sera inoculated with gibbon or orangutan HBV carrier sera grouped with HBV from gibbon and orangutan sera determined prior to inoculation. Nucleotide comparison between HBV in mouse sera and the HBV strain used for inoculation showed 100% identity.

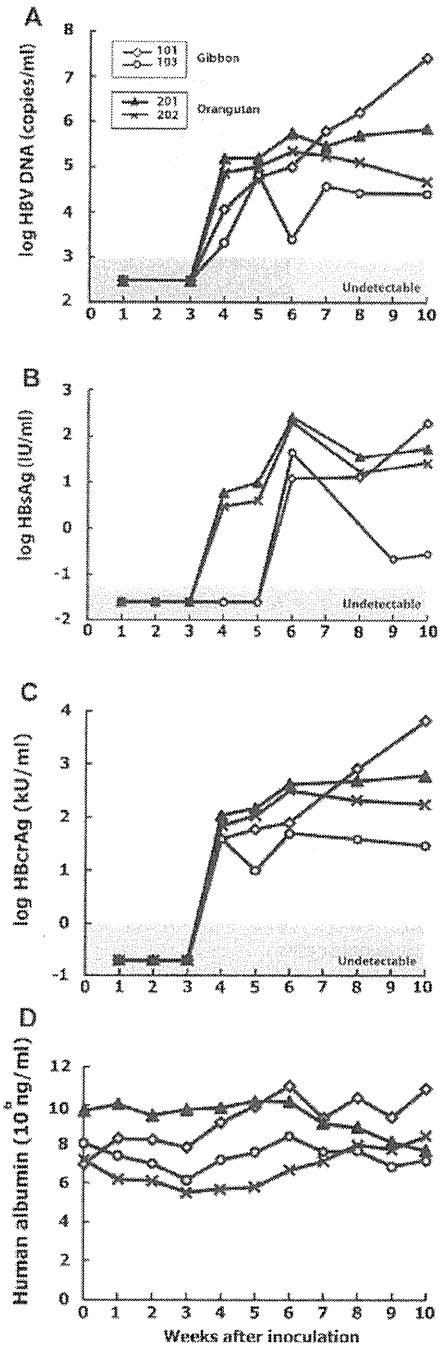

Fig. 1. HBV DNA, HBsAg, HBcrAg, and human albumin concentration in inoculated mouse sera on secondary inoculation. (A) Serum HBV DNA level. Gray zone indicates an area below the minimum sensitivity of real-time PCR (<10^3 copies/ml) (B) HBsAg concentration. The limitation of the test is 0.05 IU/ml. (C) HBcrAg level with the limited sensitivity at 1 kU/ml and (D) h-Alb concentration.

HBV infection depends on the infectious doses of HBV inoculums and host factors. In our experiment, one SCID mouse with human hapatocytes could not be infected with non-human primate HBV. This mouse lacks T- and B-lymphocytes as a protection from viral infection but still, it remains clear from viral infection. Some

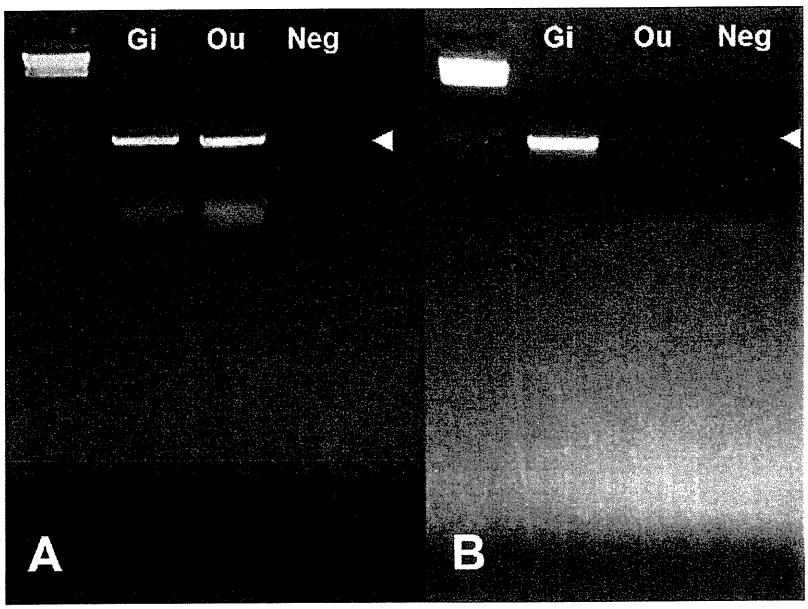

Fig. 2. CccDNA detection in liver (A) and sera (B) of mice that infected with gibbon HBV (Gi) or orangutan HBV (Ou). Neg represents negative PCR control (lacking DNA template). Arrow represents the target cccDNA PCR product.

researchers have attributed this to innate immunity of SCID mice (Lin et al., 1998). SCID mice have a normal innate immune system such as monocytes and macrophages (Ansell and Bancroft, 1989) which probably plays an important role in these mice. Moreover, infection of human hepatocytes with non-human primate HBV may be difficult due to the higher infectious dose required. Moreover, research on the early step of non-human primate HBV attachment to human hepatocytes has not been performed and the pathway of non-human primate HBV infection is still unclear. In comparison with human HBV, it might not be easy for non-human primate HBV to infect human hepatocytes.

Notably, a previous study has reported a new human HBV genotype (HBV-J) isolated from a Japanese patient with hepatocellular carcinoma (Tatematsu et al., 2009). The first HBV strain of interspecies HBV genotype J was closely related to gibbon and orangutan HBV strains and had a deletion of 33 nucleotides at the *preS1* region identical to non-human primate strains. Interestingly, this patient used to live in Borneo—a gibbon and orangutan habitat and hence, an endemic area (Tatematsu et al., 2009). He may have been infected with non-human primate HBV either by close contact or by eating raw meat of non-human primate HBV carriers (personal communication). However, infection of humans with non-human

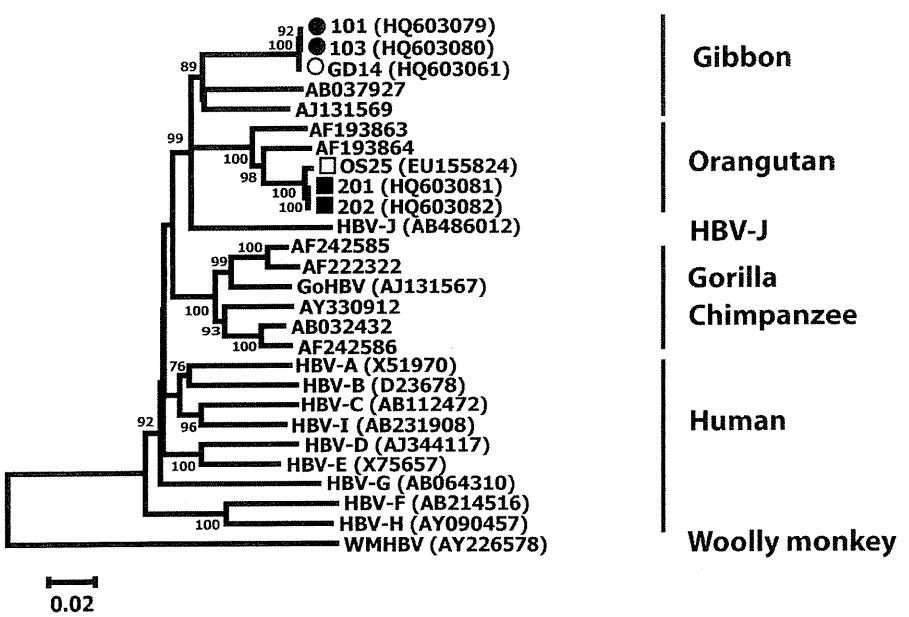

Fig. 3. Phylogenetic analysis of the entire HBV sequence obtained from mouse sera and available sequences of non-human primate HBV strains from GenBank database. Support of each branch as determined from 1000 bootstrap samples. Only 75% bootstrap values are indicated at each node. The scale bar at the bottom represents the genetic distance. Non-human primate HBV sequences obtained from our study are indicated by symbol (gibbon, ○; orangutan, □). HBV sequences obtained from mouse sera were ● and ■ for mice inoculated with gibbon and orangutan sera, respectively.

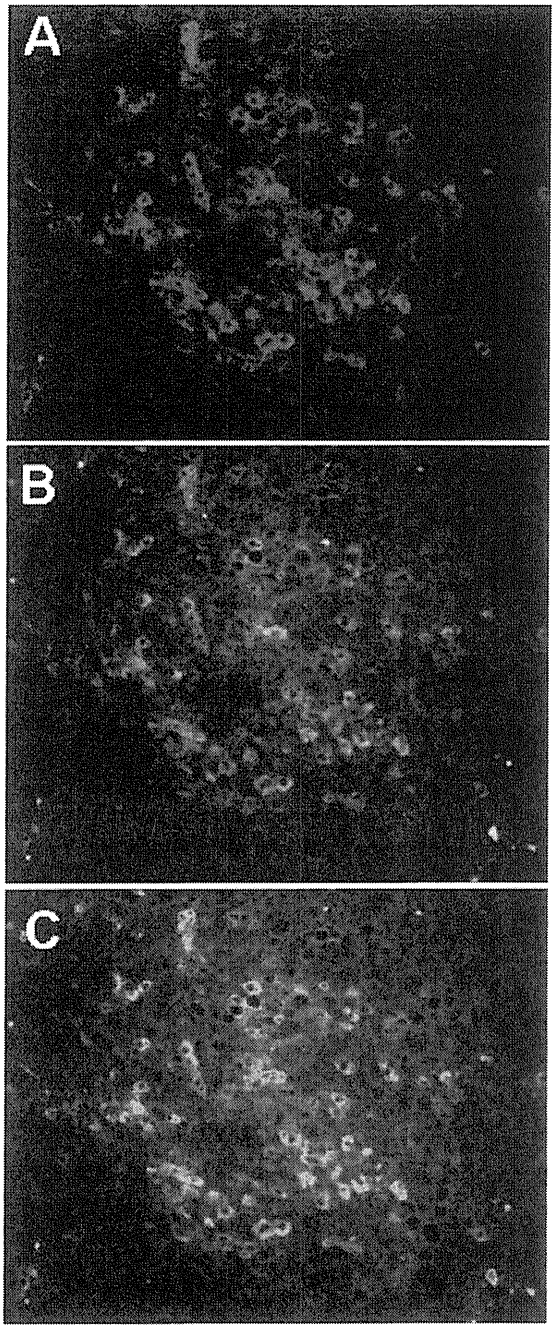

Fig. 4. Immunohistofluorescence of SCID mice infected with gibbon HBsAg-positive serum. Mouse liver tissue incubated for HBcAg (A), human albumin (B), and co-localization of HBcAg and human albumin (C).

primate HBV by eating raw meat or close contact with non-human primate HBV carriers would be hypothesis.

Yet, it has been reported that chimeric SCID mice with human hepatocytes can be infected by inoculation with HBV positive chimpanzee sera (Tabuchi et al., 2008) similar to what has been found in this study. In that previous study, human hepatocyte transplanted chimeric mice were used to study the HBV infectious titer in sera of pre-acute and late acute phase patients. These mice were inoculated with HBV infected chimpanzee sera. The chimeric mice also displayed HBV infection markers such as HBsAg, anti-HBc and anti-HBs as has been shown in this research. But the HBV in chimpanzee sera used to inoculate chimeric mice was human HBV, in contrast to the non-human primate HBV used in this study. Thus, this study is the first scientific evidence to prove and confirm that non-human primate such as gibbon and orangutan HBV can infect and replicate in human hepatocytes. Moreover, this finding can support the discovery of the HBV-J genotype which was found in the human and the assumption that humans can be infected with non-human primate HBV strains is still hypothesis.

Even though uPA-SCID mice with human hepatocytes constitute a useful animal model to study cross-species transmission, this model does not mirror the humoral and cellular immune response of the natural host. In real life, humans may be infected with non-human primate HBV and may clear this virus by their immune system. However, the results of this study indicated that human hepatocytes of chimeric mice have been infected with HBV from gibbon, orangutan and also with human HBV from infected chimpanzee sera as previously reported (Tabuchi et al., 2008). Previous studies have demonstrated cross-species transmission of human HBV to non-human primates, of non-human primate HBV to other species of non-human primates, and this study has demonstrated that non-human primate HBV can replicate in human hepatocytes. As non-human primates represent various virus reservoirs, not only of HBV but also lymphocryptovirus (LCV), Epstein-Barr virus (EBV), or simian foamy virus (SFV), people in close contact with animal HBV carriers should be aware and protect themselves from animal bites or exposure to infected blood or body fluids of non-human primates.

Acknowledgements

This research was supported by a grant-in-aid from the Ministry of Education, Culture, Sports, Science, and Technology and a grant-in-aid from the Ministry of Health, Labour, and Welfare of Japan, Takeda Science Foundation, the Department of Virology & liver Unit, Nagoya City University Graduate School of Medical Sciences, Japan, the exchange program fellowship under the program "Strategic Scholarship for Frontier Research Network" of Thailand's Commission on Higher Education, the Center of Excellence in Clinical Virology, Chulalongkorn University, the Chulalongkorn University Graduate Scholarship to Commemorate the 72nd Anniversary of His Majesty King Bhumibol Adulyadej, the Postdoctoral Fellowship, the National Research University Project of CHE (HR1155A) and Ratchadaphiseksomphot Endowment Fund.

We would like to thank the veterinary doctors and staff of the Dusit zoo, Krabok Koo and Khao Pratubchang Wildlife Breeding Center for sera and taking care of all those non-human primates. We also would like to thank Ms. Kanako Tatematsu, Ms. Hatsue Naganuma, and the entire staff of the Center of Excellence in Clinical Virology, Faculty of Medicine, Chulalongkorn University, Thailand and the Department of Virology & Liver Unit, Nagoya City University Graduate School of Medical Sciences, Nagoya City University, Japan for their assistance. Finally, we would like to thank Ms. P. Hirsch for reviewing the manuscript.

References

Abe, A., Inoue, K., Tanaka, T., Kato, J., Kajiyama, N., Kawaguchi, R., Tanaka, S., Yoshiba, M., Kohara, M., 1999. Quantitation of hepatitis B virus genomic DNA by real-time detection PCR. J. Clin. Microbiol. 37, 2899–2903.

Alter, H.J., Purcell, R.H., Gerin, J.L., London, W.T., Kaplan, P.M., McAuliffe, V.J., Wagner, J., Holland, P.V., 1977. Transmission of hepatitis B to chimpanzees by hepatitis B surface antigen-positive saliva and semen. Infect. Immun. 16, 928–933.

Ansell, J.D., Bancroft, G.J., 1989. The biology of the SCID mutation. Immunol. Today 10, 322–325.

Bancroft, W.H., Snitbhan, R., Scott, R.M., Tingpalapong, M., Watson, W.T., Tanticharoenyos, P., Karwacki, J.J., Srimarut, S., 1977. Transmission of hepatitis B virus to gibbons by exposure to human saliva containing hepatitis B surface antigen. J. Infect. Dis. 135, 79–85.

Dandri, M., Burda, M.R., Török, E., Pollok, J.M., Iwanska, A., Sommer, G., Rogiers, X., Rogler, C.E., Gupta, S., Will, H., Greten, H., Petersen, J., 2001. Repopulation of

mouse liver with human hepatocytes and in vivo infection with hepatitis B virus. Hepatology 33, 981–988.
Ganem, D., Prince, A.M., 2004. Hepatitis B virus infection—natural history and clinical consequences. N. Engl. J. Med. 350, 1118–1129.
Grethe, S., Heckel, J.O., Rietschel, W., Hufert, F.T., 2000. Molecular epidemiology of hepatitis B virus variants in nonhuman primates. J. Virol. 74, 5377–5381.
Hu, X., Margolis, H.S., Purcell, R.H., Ebert, J., Robertson, B.H., 2000. Identification of hepatitis B virus indigenous to chimpanzees. Proc. Natl. Acad. Sci. U.S.A. 97, 1661–1664.
Kim, S.H., Kim, S.H., Oh, H.K., Ryu, C.J., Park, S.Y., Hong, H.J., 2008. In vivo hepatitis B virus-neutralizing activity of an anti-HBsAg humanized antibody in chimpanzees. Exp. Mol. Med. 40, 145–149.
Kimura, T., Ohno, N., Terada, N., Rokuhara, A., Matsumoto, A., Yagi, S., Tanaka, E., Kiyosawa, K., Ohno, S., Maki, N., 2005. Hepatitis B virus DNA-negative dane particles lack core protein but contain a 22-kDa precore without C-terminal arginine-rich domain. J. Biol. Chem. 280, 21713–21719.
Kimura, T., Rokuhara, A., Sakamoto, Y., Yagi, S., Tanaka, E., Kiyosawa, K., Maki, N., 2002. Sensitive enzyme immunoassay for hepatitis B virus core-related antigens and their correlation to virus load. J. Clin. Microbiol. 40, 439–445.
Kneteman, N.M., Mercer, D.F., 2005. Mice with chimeric human livers: who says supermodels have to be tall? Hepatology 41, 703–706.
Kramvis, A., Kew, M., François, G., 2005. Hepatitis B virus genotypes. Vaccine 23, 2409–2423.
Lavanchy, D., 2004. Hepatitis B virus epidemiology, disease burden, treatment, and current and emerging prevention and control measures. J. Viral. Hepat. 11, 97–107.
Lee, W.M., 1997. Hepatitis B virus infection. N. Engl. J. Med. 337, 1733–1745.
Lin, Y.L., Liao, C.L., Chen, L.K., Yeh, C.T., Liu, C.I., Ma, S.H., Huang, Y.Y., Huang, Y.L., Kao, C.L., King, C.C., 1998. Study of Dengue virus infection in SCID mice engrafted with human K562 cells. J. Virol. 72, 9729–9737.
MacDonald, D.M., Holmes, E.C., Lewis, J.C., Simmonds, P., 2000. Detection of hepatitis B virus infection in wild-born chimpanzees (*Pan troglodytes verus*): phylogenetic relationships with human and other primate genotypes. J. Virol. 74, 4253–4257.
Makuwa, M., Souquière, S., Telfer, P., Leroy, E., Bourry, O., Rouquet, P., Clifford, S., Wickings, E.J., Roques, P., Simon, F., 2003. Occurrence of hepatitis viruses in wild-born non-human primates: a 3 year (1998–2001) epidemiological survey in Gabon. J. Med. Primatol. 32, 307–314.
Mason, A.L., Xu, L., Guo, L., Kuhns, M., Perrillo, R.P., 1998. Molecular basis for persistent hepatitis B virus infection in the liver after clearance of serum hepatitis B surface antigen. Hepatology 27, 1736–1742.
Mason, W.S., Burrell, C.J., Casey, J., Gerlich, W.H., Howard, C.R., Kann, M., Lanford, R., Newbold, J., Schaefer, S., Taylor, J.M., Will, H., 2005. The DNA and RNA transcribing viruses. In: Fauquet, C.M., Mayo, M.A., Maniloff, J., Desselberger, U., Ball, L.A. (Eds.), Virus Taxonomy. Eighth Report of the International Committee on Taxonomy of Viruses. Elsevier/Academic Press, London, pp. 371–382.
McQuillan, G.M., Townsend, T.R., Fields, H.A., Carroll, M., Leahy, M., Polk, B.F., 1989. Seroepidemiology of hepatitis B virus infection in the United States. 1976 to 1980. Am. J. Med. 87, 5S–10S.
Mercer, D.F., Schiller, D.E., Elliott, J.F., Douglas, D.N., Hao, C., Rinfret, A., Addison, W.R., Fischer, K.P., Churchill, T.A., Lakey, J.R., Tyrrell, D.L., Kneteman, N.M., 2001. Hepatitis C virus replication in mice with chimeric human livers. Nat. Med. 7, 927–933.
Meuleman, P., Libbrecht, L., De Vos, R., de Hemptinne, B., Gevaert, K., Vandekerckhove, J., Roskams, T., Leroux-Roels, G., 2005. Morphological and biochemical characterization of a human liver in a uPA-SCID mouse chimera. Hepatology 41, 847–856.
Mimms, L.T., Solomon, L.R., Ebert, J.W., Fields, H., 1993. Unique preS sequence in a gibbon-derived hepatitis B virus variant. Biochem. Biophys. Res. Commun. 195, 186–191.
Nopporpanth, S., Haagmans, B.L., Bhattarakosol, P., Ratanakorn, P., Niesters, H.G., Osterhaus, A.D., Poovorawan, Y., 2003. Molecular epidemiology of gibbon hepatitis B virus transmission. J. Gen. Virol. 84, 147–155.
Petersen, J., Dandri, M., Gupta, S., Rogler, C.E., 1998. Liver repopulation with xenogenic hepatocytes in B and T cell-deficient mice leads to chronic hepadnavirus infection and clonal growth of hepatocellular carcinoma. Proc. Natl. Acad. Sci. U.S.A. 95, 310–315.
Robertson, B.H., 2001. Viral hepatitis and primates: historical and molecular analysis of human and nonhuman primate hepatitis A, B, and the GB-related viruses. J. Viral. Hepat. 8, 233–242.
Rokuhara, A., Sun, X., Tanaka, E., Kimura, T., Matsumoto, A., Yao, D., Yin, L., Wang, N., Maki, N., Kiyosawa, K., 2005. Hepatitis B virus core and core-related antigen quantitation in Chinese patients with chronic genotype B and C hepatitis B virus infection. J. Gastroenterol. Hepatol. 20, 1726–1730.
Rokuhara, A., Tanaka, E., Matsumoto, A., Kimura, T., Yamaura, T., Orii, K., Sun, X., Yagi, S., Maki, N., Kiyosawa, K., 2003. Clinical evaluation of a new enzyme immunoassay for hepatitis B virus core-related antigen; a marker distinct from viral DNA for monitoring lamivudine treatment. J. Viral. Hepat. 10, 324–330.
Sall, A.A., Starkman, S., Reynes, J.M., Lay, S., Nhim, T., Hunt, M., Marx, N., Simmonds, P., 2005. Frequent infection of *Hylobates pileatus* (pileated gibbon) with species-associated variants of hepatitis B virus in Cambodia. J. Gen. Virol. 86, 333–337.
Sa-nguanmoo, P., Thongmee, C., Ratanakorn, P., Pattanarangsan, R., Boonyarittichaikij, R., Chodapisitkul, S., Theamboonlers, A., Tangkijvanich, P., Poovorawan, Y., 2008. Prevalence, whole genome characterization and phylogenetic analysis of hepatitis B virus in captive orangutan and gibbon. J. Med. Primatol. 37, 277–289.
Scott, R.M., Snitbhan, R., Bancroft, W.H., Alter, H.J., Tingpalapong, M., 1980. Experimental transmission of hepatitis B virus by semen and saliva. J. Infect. Dis. 142, 67–71.
Sharma, S.K., Saini, N., Chwla, Y., 2005. Hepatitis B virus: inactive carriers. Virol. J. 2, 82.
Shinkai, N., Tanaka, Y., Orito, E., Ito, K., Ohno, T., Hirashima, N., Hasegawa, I., Sugauchi, F., Ueda, R., Mizokami, M., 2006. Measurement of hepatitis B virus core-related antigen as predicting factor for relapse after cessation of lamivudine therapy for chronic hepatitis B virus infection. Hepatol. Res. 36, 272–276.
Starkman, S.E., MacDonald, D.M., Lewis, J.C., Holmes, E.C., Simmonds, P., 2003. Geographic and species association of hepatitis B virus genotypes in non-human primates. Virology 314, 381–393.
Sugauchi, F., Mizokami, M., Orito, E., Ohno, T., Kato, H., Suzuki, S., Kimura, Y., Ueda, R., Butterworth, L.A., Cooksley, W.G., 2001. A novel variant genotype C of hepatitis B virus identified in isolates from Australian Aborigines: complete genome sequence and phylogenetic relatedness. J. Gen. Virol. 82, 883–892.
Sugiyama, M., Tanaka, Y., Kato, T., Orito, E., Ito, K., Acharya, S.K., Gish, R.G., Kramvis, A., Shimada, T., Izumi, M., Kaito, M., Miyakawa, Y., Mizokami, M., 2006. Influence of hepatitis B virus genotypes on the intra- and extracellular expression of viral DNA and antigens. Hepatology 44, 915–924.
Sugiyama, M., Tanaka, Y., Kurbanov, F., Maruyama, I., Shimada, T., Takahashi, S., Shirai, T., Hino, K., Sakaida, I., Mizokami, M., 2009. Direct cytopathic effects of particular hepatitis B virus genotypes in severe combined immunodeficiency transgenic with urokinase-type plasminogen activator mouse with human hepatocytes. Gastroenterology 136, 652–662.
Suzuki, F., Miyakoshi, H., Kobayashi, M., Kumada, H., 2009. Correlation between serum hepatitis B virus core-related antigen and intrahepatic covalently closed circular DNA in chronic hepatitis B patients. J. Med. Virol. 81, 27–33.
Tabor, E., FrÖsner, G., Deinhardt, F., Gerety, R.J., 1980. Hepatitis B e antigen and antibody: detection by radioimmunoassay in chimpanzees during experimental hepatitis B. J. Med. Virol. 6, 91–99.
Tabuchi, A., Tanaka, J., Katayama, K., Mizui, M., Matsukura, H., Yugi, H., Shimada, T., Miyakawa, Y., Yoshizawa, H., 2008. Titration of hepatitis B virus infectivity in the sera of pre-acute and late acute phases of HBV infection: transmission experiments to chimeric mice with human liver repopulated hepatocytes. J. Med. Virol. 80, 2064–2068.
Takahashi, K., Brotman, B., Usuda, S., Mishiro, S., Prince, A.M., 2000. Full-genome sequence analyses of hepatitis B virus (HBV) strains recovered from chimpanzees infected in the wild: implications for an origin of HBV. Virology 267, 58–64.
Tatematsu, K., Tanaka, Y., Kurbanov, F., Sugauchi, F., Mano, S., Maeshiro, T., Nakayoshi, T., Wakuta, M., Miyakawa, Y., Mizokami, M., 2009. A genetic variant of hepatitis B virus divergent from known human and ape genotypes isolated from a Japanese patient and provisionally assigned to new genotype J. J. Virol. 83, 10538–10547.
Tateno, C., Yoshizane, Y., Saito, N., Kataoka, M., Utoh, R., Yamasaki, C., Tachibana, A., Soeno, Y., Asahina, K., Hino, H., Asahara, T., Yokoi, T., Furukawa, T., Yoshizato, K., 2004. Near completely humanized liver in mice shows human-type metabolic responses to drugs. Am. J. Pathol. 165, 901–912.
Warren, K.S., Niphuis, H., Heriyanto, Verschoor, E.J., Swan, R.A., Heeney, J.L., 1998. Seroprevalence of specific viral infections in confiscated orangutans (*Pongo pygmaeus*). J. Med. Primatol. 27, 33–37.
Wong, D.K., Tanaka, Y., Lai, C.L., Mizokami, M., Fung, J., Yuen, M.F., 2007. Hepatitis B virus core-related antigens as markers for monitoring chronic hepatitis B infection. J. Clin. Microbiol. 45, 3942–3947.

TANK-binding kinase 1 (TBK1) controls cell survival through PAI-2/serpinB2 and transglutaminase 2

Mireille Delhase[a,b,c,d,1], Soo-Youl Kim[e,2], Ho Lee[f,2], Aya Naiki-Ito[g,2], Yi Chen[c,3], Eu-Ree Ahn[e], Kazuhiro Murata[d], Se-Jin Kim[e], Norman Lautsch[a,4], Koichi S. Kobayashi[a,h], Tomoyuki Shirai[g], Michael Karin[c,1,5], and Makoto Nakanishi[d,5]

[a]Department of Cancer Immunology and AIDS, Dana-Farber Cancer Institute, Boston, MA 02115; [b]Department of Pathology, Harvard Medical School, Boston, MA 02115; [c]Laboratory of Gene Regulation and Signal Transduction, Department of Pharmacology, School of Medicine, University of California at San Diego, La Jolla, CA 92093-0723; [d]Department of Cell Biology, Graduate School of Medical Sciences, Nagoya City University, Nagoya 467-8601, Japan; [e]Cancer Cell and Molecular Biology Branch and [f]Cancer Experimental Resources Branch, Division of Cancer Biology, Research Institute, National Cancer Center, Goyang 410-769, Republic of Korea; [g]Department of Experimental Pathology and Tumor Biology, Graduate School of Medical Sciences, Nagoya City University, Nagoya 467-8601, Japan; and [h]Department of Microbiology and Immunology, Harvard Medical School, Boston, MA 02115

Contributed by Michael Karin, November 30, 2011 (sent for review October 5, 2011)

The decision between survival and death in cells exposed to TNF relies on a highly regulated equilibrium between proapoptotic and antiapoptotic factors. The TNF-activated antiapoptotic response depends on several transcription factors, including NF-κB and its RelA/p65 subunit, that are activated through phosphorylation-mediated degradation of IκB inhibitors, a process controlled by the IκB kinase complex. Genetic studies in mice have identified the IκB kinase-related kinase TANK-binding kinase 1 (TBK1; also called NAK or T2K) as an additional regulatory molecule that promotes survival downstream of TNF, but the mechanism through which TBK1 exerts its survival function has remained elusive. Here we show that TBK1 triggers an antiapoptotic response by controlling a specific RelA/p65 phosphorylation event. TBK1-induced RelA phosphorylation results in inducible expression of plasminogen activator inhibitor-2 (PAI-2), a member of the serpin family with known antiapoptotic activity. PAI-2 limits caspase-3 activation through stabilization of transglutaminase 2 (TG2), which cross-links and inactivates procaspase-3. Importantly, *Tg2*$^{-/-}$ mice were found to be more susceptible to apoptotic cell death in two models of TNF-dependent acute liver injury. Our results establish PAI-2 and TG2 as downstream mediators in the antiapoptotic response triggered upon TBK1 activation.

apoptosis | tumor necrosis factor signaling | transcriptional regulation | posttranslational protein modification

Apoptosis is a highly regulated cell death process that controls cellular homeostasis and prevents survival of injured, damaged, or transformed cells (1). Apoptosis depends on a proteolytic cascade involving intracellular proteases, known as caspases, that are activated in response to cell-intrinsic and -extrinsic insults (2). The proinflammatory cytokine TNF can trigger apoptosis through its main cell surface receptor, TNF receptor (TNFR) type 1 (TNFR1) (3, 4). Engagement of TNFR1 results in assembly of multiprotein signaling complexes around its cytoplasmic death domain, leading to activation of caspase-8, which in turns activates the executioner caspase-3 that ultimately mediates cell death (3, 4). TNF-induced apoptosis is prevented by rapid activation of the IκB kinase (IKK) complex and subsequently NF-κB. NF-κB antagonizes apoptosis and maintains cell survival through induction of antiapoptotic genes encoding factors that tightly control caspase activation, such as members of the cellular inhibitor of apoptosis family (cIAP), the cellular FLICE inhibitory protein, and Bfl-1/A1, a member of the prosurvival Bcl-2 family (5, 6). Besides this intrinsic survival pathway, additional autocrine cascades activated through release of cytokines, such as TGF-α, provide additional prosurvival signals, suggesting the existence of yet unexplored feedback loops controlling cell-fate decisions (7).

TANK-binding kinase 1 (TBK1; also called NAK or T2K) was proposed to serve as an NF-κB activator (8, 9). TBK1 was originally found to interact with the TNFR- associated factor (TRAF) binding protein TANK and form, with TRAF2, a ternary complex able to activate NF-κB in a kinase-dependent manner (8). In addition, TBK1 was found to be recruited to TNFR1 upon TNF binding (10). Mice deficient in TBK1 die during embryonic development from massive liver apoptosis (11, 12), a phenotype also exhibited by mice lacking the NF-κB subunit RelA/p65 or critical components (IKKβ and IKKγ/NEMO) of the IKK complex (13). Embryonic lethality in *Tbk1*$^{-/-}$ mice was confirmed to be TNF-dependent, as these mice survive upon deletion of TNFRI (11). However, characterization of *Tbk1*$^{-/-}$ mice failed to explain how TBK1 contributes to NF-κB–dependent gene expression (11), and the mechanism by which TBK1 controls NF-κB activity to exert its antiapoptotic function has remained elusive.

In the present study, we have readdressed the function of TBK1 in TNF-mediated NF-κB activation by using a systematic approach aimed at identifying and characterizing NF-κB–dependent genes activated in a TBK1-dependent manner that encode potential antiapoptotic factors. Defective expression of such genes may account, at least in part, for TNF-induced liver failure in *Tbk1*$^{-/-}$ embryos. We now show that TBK1 controls the expression of plasminogen activator inhibitor-2 (PAI-2), a member of the ov-serpin family (14). PAI-2 maintains survival of TNF-stimulated cells through the protein modifier transglutaminase 2 (TG2), a pleiotropic enzyme able to cross-link procaspase-3 into inactive dimers. Our data support an unexplored regulatory mechanism in the TNF-activated pathway.

Results

TBK1 Controls TNF-Mediated NF-κB Activation Through RelA Ser^{534} Phosphorylation. We used a pool of spontaneously immortalized mouse embryonic fibroblasts (MEFs) derived from WT and *Tbk1*$^{-/-}$ mice to understand how TBK1 prevents apoptosis. *Tbk1*$^{-/-}$ cells were more sensitive to TNF-induced apoptosis than WT cells when challenged for 24 h, and this was further enhanced in the presence of the protein synthesis inhibitor cycloheximide (CHX) (Fig. 1*A*). Enhanced TNF-induced apoptosis

Author contributions: M.D., M.K., and M.N. designed research; M.D., H.L., A.N.-I., E.-R.A., K.M., and S.-J.K. performed research; Y.C., N.L., K.S.K., and T.S. contributed new reagents/analytic tools; M.D., S.-Y.K., M.K., and M.N. analyzed data; and M.D. and M.K. wrote the paper.

The authors declare no conflict of interest.

[1]To whom correspondence may be addressed. E-mail: mdelhase@gmail.com or karinoffice@ucsd.edu.

[2]S.-Y.K., H.L., and A.N.-I. contributed equally to this work.

[3]Present address: Shanghai Kanda Biotechnology, Shanghai 201203, China.

[4]Present address: Department of Integrative Physiology and Metabolism, Joslin Diabetes Center, Boston, MA 02115.

[5]M.K. and M.N. contributed equally to this work.

See Author Summary on page 1005.

This article contains supporting information online at www.pnas.org/lookup/suppl/doi:10.1073/pnas.1119296109/-/DCSupplemental.

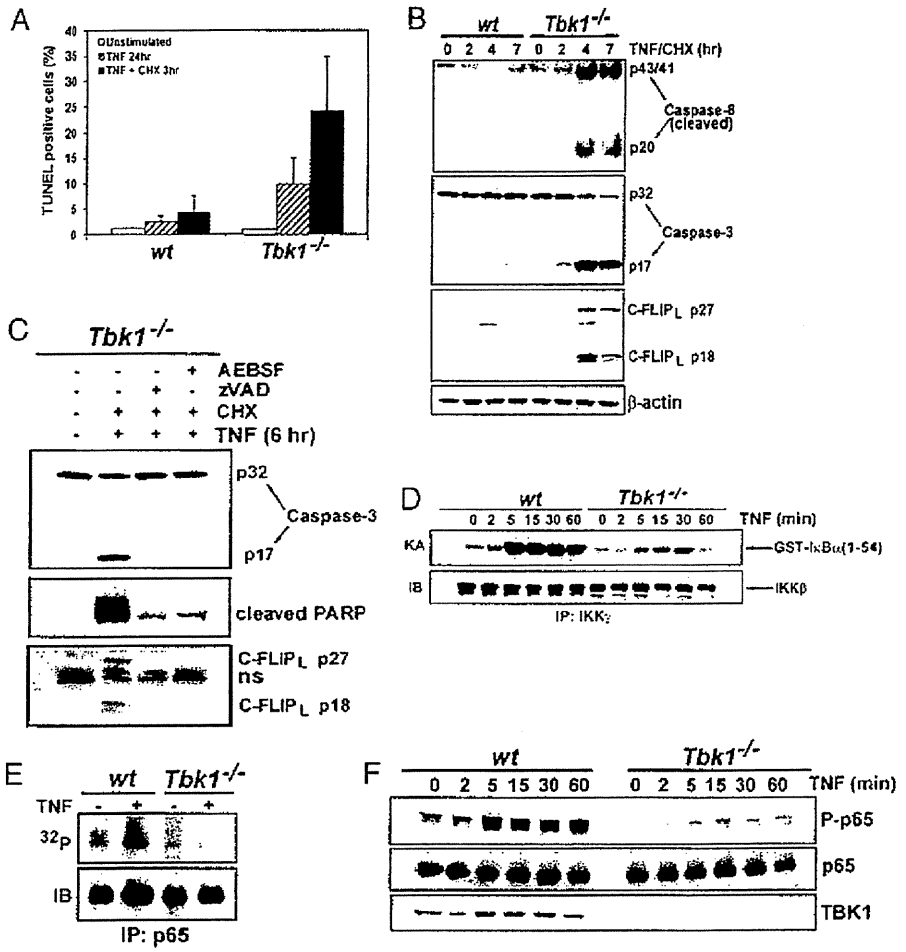

Fig. 1. TBK1 protects MEFs from TNF-induced apoptosis and modulates IKK-dependent phosphorylation of RelA/p65. (*A*) Wt and *Tbk1*$^{-/-}$ MEFs were treated for 24 h with TNF (25 ng/mL) alone or for 3 h with TNF in the presence of CHX (10 μg/mL). Apoptotic cells were detected by TUNEL assays. The bars represent averages ± SD of three different experiments. Approximately 1,200 cells were counted in each experiment. (*B*) MEFs treated with TNF and CHX for the indicated times were analyzed for caspase-8 and caspase-3 activation by immunodetection of their cleaved forms. (*C*) Cell extracts prepared from *Tbk1*$^{-/-}$ MEFs treated for 6 h with TNF and CHX in the presence of z-VAD-FMK (20 μM), AEBSF (0.5 mM), or DMSO (vehicle) were analyzed by immunoblotting for caspase-3 activation and PARP cleavage. (*D*) IKK activity in TNF-treated MEFs was measured by immunocomplex kinase assay using GST-IκBα(1-54) as a substrate (19). (*E*) RelA phosphorylation was examined after its immunoprecipitation from [^{32}P]orthophosphate-labeled and TNF-stimulated MEFs. Phospho-RelA was detected by autoradiography and the total amount of RelA by immunoblotting (IB). (*F*) Phosphorylation of RelA was examined by immunoblotting using a phospho-specific huRelA(Ser^{536}) antibody.

was associated with elevated caspase-8 and caspase-3 activation in *Tbk1*$^{-/-}$ MEFs (Fig. 1*B*). Caspase-dependent cleavage of cFLIP$_L$, the cellular inhibitor of caspase-8, was also observed in *Tbk1*$^{-/-}$, and not in WT, MEFs (Fig. 1*B*), but cFLIP expression, which depends on NF-κB, remained unchanged (Fig. 2*C* and Fig. S1). TNF-induced apoptosis as determined by cleavage of poly(ADP-ribose) polymerase (PARP), caspase-3, and cFLIP$_L$, was prevented by treatment of *Tbk1*$^{-/-}$ MEFs with the pan-caspase inhibitor carbobenzoxy-valyl-alanyl-aspartyl-[O-methyl]-fluoromethylketone (z-VAD-FMK) or the serine protease inhibitor 4-(2-aminoethyl) benzenesulfonyl fluoride, AEBSF (Fig. 1*C*). Amounts of several other antiapoptotic proteins, including c-IAP1, c-IAP2, Bcl-2, and Bcl-X$_L$, were not substantially reduced in *Tbk1*$^{-/-}$ MEFs (Fig. S1).

In addition to NF-κB and caspases, TNF activates MAPKs c-Jun NH_2-terminal kinase (JNK), p38, and ERK (15). Instead of being strongly enhanced as in RelA- or IKKβ-deficient cells (16), JNK and p38 activities were somewhat reduced in *Tbk1*$^{-/-}$ MEFs (Fig. S2*A*). However, activation of the JNK-regulated transcription factors c-Jun and ATF-2 through phosphorylation and nuclear translocation was not affected by TBK1 ablation (Fig. S2*B*). Phosphorylation of nuclear CREB, a target for p38, was also normal. Interestingly, IKK activation was reduced in TNF-stimulated *Tbk1*$^{-/-}$ MEFs compared with WT cells (Fig. 1*D*). This is consistent with our previous observation that TBK1 could activate IKK in vitro (9). However, in agreement with a previous report (11), IκBα and IκBβ were phosphorylated and degraded normally in TNF-stimulated *Tbk1*$^{-/-}$ MEFs (Fig. S3*A*), but delayed IκB resynthesis was observed, suggesting a possible defect in NF-κB–directed transcription. Nuclear accumulation of RelA, p50, and c-Rel appeared to be normal in *Tbk1*$^{-/-}$ MEFs (Fig. S3 *B* and *C*), and so was the binding of RelA to its target gene promoters (Fig. S3*D*).

TBK1 can phosphorylate RelA in vitro (17, 18). Therefore, we examined the role of TBK1 in RelA phosphorylation in living cells. Endogenous RelA, immunoprecipitated from untreated and TNF-stimulated WT MEFs, was labeled with [^{32}P]orthophosphate. TNF stimulated phosphorylation of RelA in WT cells (Fig. 1*E* and Fig. S4*A*), but both basal and induced RelA phosphorylations were diminished in *Tbk1*$^{-/-}$ MEFs (Fig. 1*E*). Experiments performed in MEFs defective for individual IKK

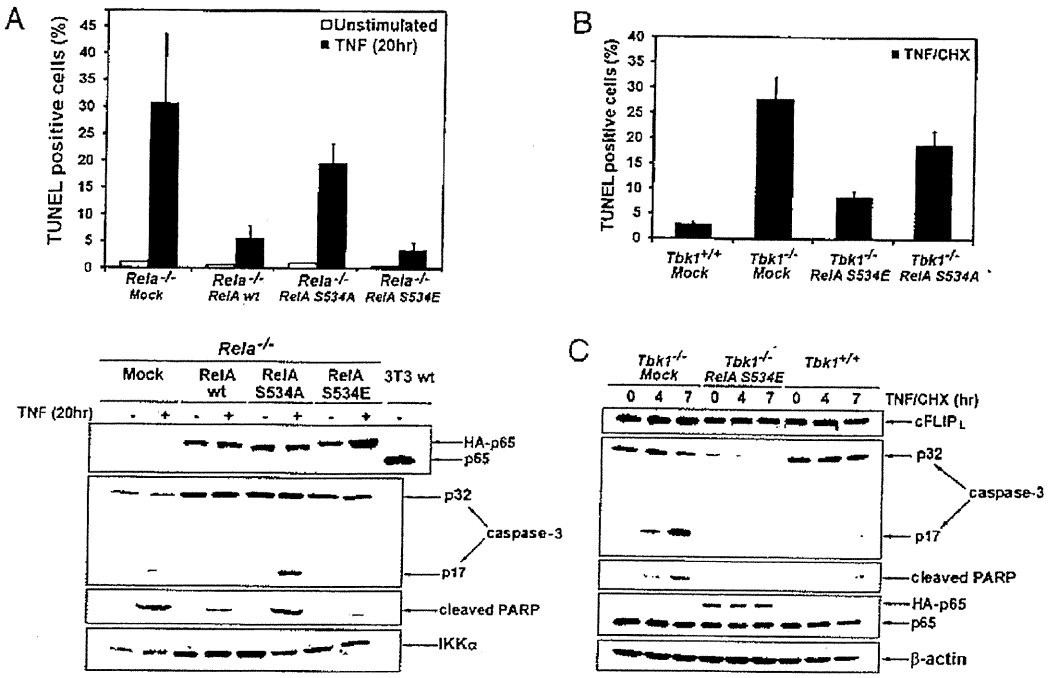

Fig. 2. Phospho-RelA protects MEFs from TNF-induced apoptosis. (*A*) *Rela*$^{-/-}$ MEFs infected with an empty retrovirus (mock) or retroviruses expressing HA-tagged wt RelA, RelA(S534A), or RelA(S534E) were left unstimulated or were treated with TNF (20 h). Apoptotic cells were detected by TUNEL staining. Represented are averages ± SD of three separate experiments. Cell lysates were analyzed for caspase-3 activation, PARP cleavage, and RelA expression by immunoblotting. (*B*) *Tbk1*$^{-/-}$ MEFs expressing RelA(S534A) or RelA(S534E) were treated for 3 h with TNF in the presence of CHX. Apoptotic cells were detected by TUNEL assay and quantified as described earlier. (*C*) Lysates were prepared from cells in *B* that were stimulated with TNF plus CHX for the indicated times. Caspase-3 activation and protein expression were determined by immunoblotting as in *A*.

subunits indicated that a functional IKK complex was also required for TNF-induced RelA phosphorylation (Fig. S5*A*). These results are consistent with our early suggestion that TBK1 stimulates NF-κB activity through the canonical IKK complex (9). By using an established peptide mapping strategy (19), the TNF-inducible phosphorylation sites were localized to a 4.6-kDa CNBr peptide located in the C-terminal transactivation domain of RelA (Fig. S4 *B* and *C*). The major TNF-inducible phosphorylation site was identified as Ser^{534} of mouse RelA (corresponding to Ser^{536} of human RelA; Fig. S4*D*). Reduced Ser^{534} phosphorylation in *Tbk1*$^{-/-}$ MEFs was confirmed by immunoblotting performed with phospho-specific RelA antibody (Fig. 1*F*). RelA Ser^{534} phosphorylation was also impaired in cells defective in both IKK catalytic subunits (Fig. S5*B*). Ser^{534} phosphorylation took place in the cytosol, as it was dramatically reduced in *IκBα*$^{-/-}$ MEFs, in which most of RelA is constitutively nuclear (Fig. S5*C*).

Ser^{534} Phosphorylation Regulates RelA Antiapoptotic Function. To examine whether phosphorylation of RelA at Ser^{534} was required to protect MEFs from TNF-induced apoptosis, a retroviral vector was used to stably express WT RelA, RelA(S534A), or a phospho-mimic RelA(S534E) mutant in *Rela*$^{-/-}$ MEFs. Expression levels were similar to that of endogenous RelA in WT MEFs (Fig. 2*A*), and all the expressed proteins underwent nuclear translocation. Whereas WT RelA and RelA(S534E) protected *Rela*$^{-/-}$ MEFs from TNF-induced apoptosis, expression of RelA(S534A) provided little protection (Fig. 2*A*). Similar results were obtained when caspase-3 activation and cleavage of PARP were examined: WT RelA and RelA(S534E) prevented caspase-3 activation, whereas RelA(S534A) did not (Fig. 2*A*). Expression of RelA(S534E) but not RelA(S534A) also prevented apoptosis (Fig. 2*B*), PARP cleavage, and caspase-3 activation (Fig. 2*C*) in *Tbk1*$^{-/-}$ MEFs. Surprisingly, the amount of procaspase-3 was dramatically reduced in *Tbk1*$^{-/-}$ MEFs expressing RelA(S534E) (Fig. 2*C*). This reduction in procaspase-3 protein amount appeared to be specific, as other proteins such as cFLIP$_L$ (Fig. 2*C*) and XIAP (Fig. 3*G*) were not affected.

TBK1 Controls TNF-Induced Expression of Survival Gene *Pai-2/serpinB2*. Genes that mediate the survival function of TBK1 were identified by microarray analysis of RNAs isolated from resting and TNF-stimulated WT and *Tbk1*$^{-/-}$ MEFs. Selected data were validated by quantitative real-time PCR (qRT-PCR). Induction of most previously described (20) NF-κB–dependent genes was not affected by TBK1 deficiency (Fig. S6). As expected, induction of genes that require activation of IFN regulatory factors in addition to NF-κB, such as *IP-10*, *Rantes*, or *Irf9* was impaired in TNF-stimulated *Tbk1*$^{-/-}$ MEFs (Fig. 3*A* and Fig. S6). Among well established antiapoptotic genes, induction of *c-Iap-1*, *c-Iap-2*, *Xiap*, and *BclX$_L$* was observed in *Tbk1*$^{-/-}$ MEFs, whereas *c-Flip* expression was constitutive and not TNF-inducible in MEFs (Fig. S6). Further examination of less studied NF-κB target genes with a documented survival function identified *Pai-2/serpinb2*, a gene encoding PAI-2, a serine protease inhibitor previously shown to inhibit TNF-induced apoptosis in cancer cells (21, 22), as a potential candidate (Fig. 3*A*). Both basal (Fig. 3*A*, *Inset*) and TNF-induced expressions of *Pai-2* were dramatically reduced in *Tbk1*$^{-/-}$ MEFs (Fig. 3*A*). However, *Pai-2* expression was restored in *Tbk1*$^{-/-}$ MEFs upon expression of RelA(S534E), whereas *IP-10* induction remained defective (Fig. 3*B*). Induction of other NF-κB–dependent genes such as *IκBα* and *iNos* was not affected (Fig. 3*B*). Reconstitution of *Tbk1*$^{-/-}$ MEFs with RelA(S534E) also increased PAI-2 protein expression (Fig. 3*C*).

The antiapoptotic function of ectopic PAI-2 reintroduced into *Tbk1*$^{-/-}$ MEFs was examined by retroviral transduction. Recon-

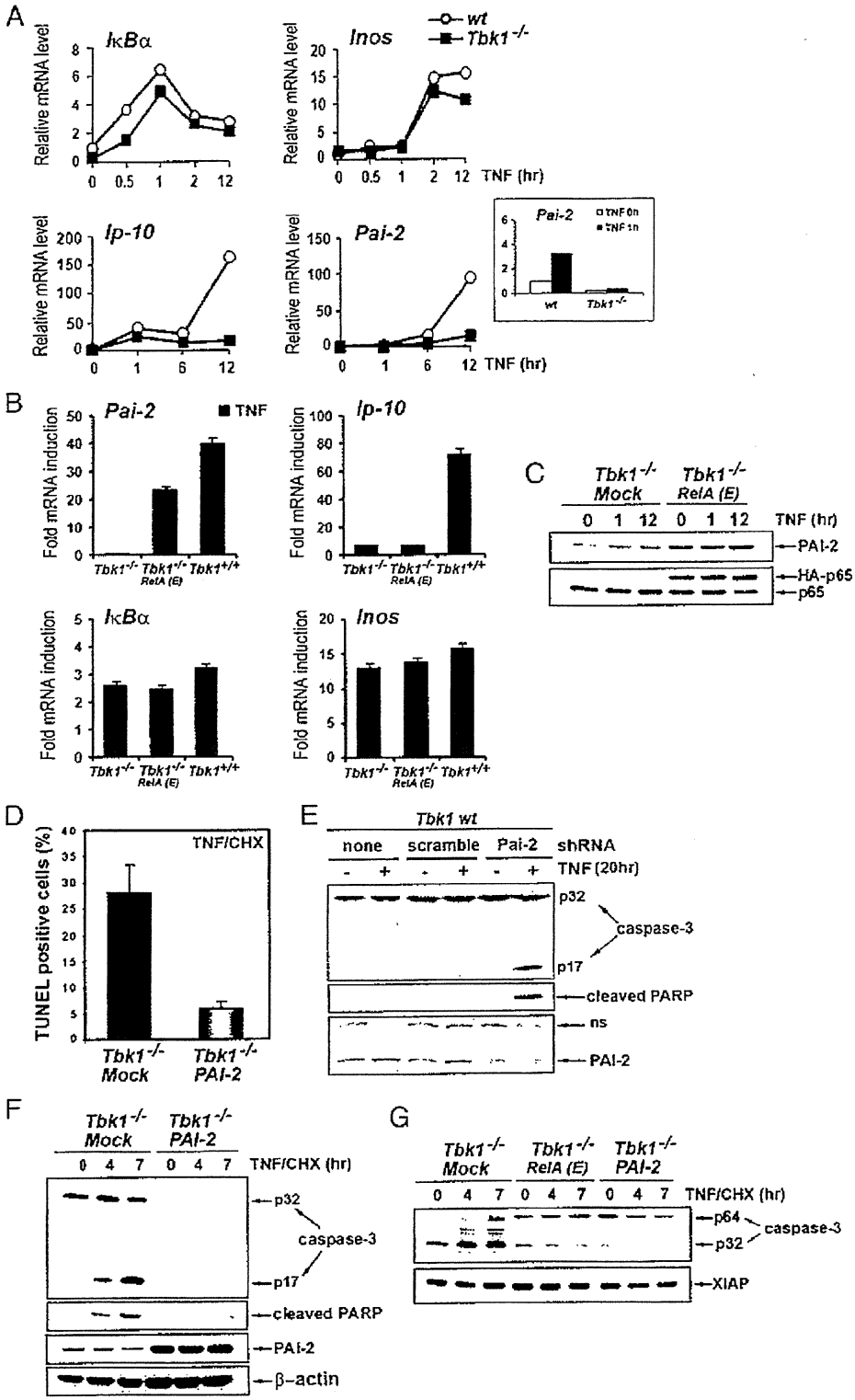

Fig. 3. TBK-1 controls NF-κB–dependent expression of the survival factor PAI-2. (*A*) Induction of NF-κB target genes was determined by qRT-PCR amplification of mRNAs prepared from WT and *Tbk1*$^{-/-}$ MEFs that were stimulated with TNF for the indicated times. *Inset*: Short time course (0 and 1 h) of *Pai-2* mRNA induction in both cell types. (*B*) Relative mRNA induction was analyzed by qRT-PCR amplification of RNAs prepared from WT (*Tbk1*$^{+/+}$), *Tbk1*$^{-/-}$, and *Tbk1*$^{-/-}$ MEFs expressing RelA(S534E), depicted as RelA(E) that were stimulated with TNF for 2 h (*IκBα*), 6 h (*Pai-2* and *Inos*), or 14 h (*Ip10*). (*C*) Expression of endogenous PAI-2 and RelA was examined by immunoblotting in extracts prepared from cells that were stimulated with TNF for the indicated times. (*D*) Apoptotic cell death, determined by TUNEL assay as described earlier, was quantified in *Tbk1*$^{-/-}$ MEFs and in cells stably expressing PAI-2 that were stimulated for 3 h with TNF in the presence of CHX. (*E*) WT MEFs expressing a *Pai-2* shRNA or a scrambled shRNA were treated with TNF for 20 h. Caspase-3 activation, PARP cleavage, and protein expression were determined by immunoblotting. (*F* and *G*) Caspase-3 activation, PARP cleavage, and protein expression were determined by immunoblotting in extracts prepared from the indicated cells that were stimulated with TNF in the presence of CHX for the indicated times.

stituted cells were protected from TNF-induced apoptosis (Fig. 3*D*) or activation of caspase-3 (Fig. 3*F*). By contrast, down-regulation of *Pai-2* expression by stably expressing a *Pai-2*-specific shRNA, but not a scrambled shRNA, potentiated TNF-induced caspase-3 activation and apoptosis in WT MEFs (Fig. 3*E*). Similarly to what was observed in *Tbk1*$^{-/-}$ MEFs expressing RelA(S534E), the amount of procaspase-3 was dramatically reduced in *Tbk1*$^{-/-}$ MEFs expressing PAI-2, and a slow-migrating form of procaspase-3 with an apparent molecular weight of 64 kDa (depicted as p64) was observed in *Tbk1*$^{-/-}$ MEFs expressing either RelA (S534E) or PAI-2 (Fig. 3*G*). A similar slow-migrating caspase-3 isoform was previously described as a cross-linked procaspase-3 in thapsigargin-treated HCT116 cancer cells and in tumor cells exposed to hypoxia (23, 24). In both cases, caspase-3 cross-linking into nonfunctional dimers or multimers is mediated by TG2, a multifunctional enzyme that induces posttranslational protein modifications by transamidation (25). TG2 was reported to have antiapoptotic function not only in vitro (23, 24) but also in vivo, as TG2-deficient mice show increased sensitivity to apoptosis induced by activation of the CD95/Fas receptor (26), a molecule related to TNFR1.

TG2 Is a TBK1-Regulated Antiapoptotic Factor. Endogenous TG2 activity was analyzed in WT and *Tbk1*$^{-/-}$ MEFs stimulated with TNF by examining incorporation of biotinylated pentylamines into cellular proteins (27). TNF induced transamidation in WT MEFs but not in *Tbk1*$^{-/-}$ MEFs (Fig. 4*A*). TNF also failed to stimulate *Tg2* gene expression in *Tbk1*$^{-/-}$ MEFs, whereas expression of *Tg1* was somehow increased in these cells (Fig. 4*B*). TG2 protein could hardly be detected in MEFs because of the poor quality of available antibodies combined with its very low level of expression. However, we could observe that basal and TNF-induced endogenous TG2 protein amounts were increased in *Tbk1*$^{-/-}$ MEFs expressing RelA(S534E) (Fig. 4*C*, *Upper*). Interestingly, basal TG2 expression was also increased in *Tbk1*$^{-/-}$ MEFs constitutively expressing PAI-2, suggesting that PAI-2 might stabilize TG2 (Fig. 4*C*, *Lower*). Similarly, MEFs treated with the proteasome inhibitor MG132 contained more TG2 protein (Fig. S7*A*), suggesting the existence of a tight post-translational control that down-regulates TG2 protein expression. Consistent with PAI-2's involvement in stabilization of TG2, an interaction between PAI-2 and TG2 was observed by coimmunoprecipitation in MEFs expressing HA-PAI-2 and human TG2 (Fig. 4*D*). We next examined whether the activity responsible for cross-linking of procaspase-3 was associated with PAI-2. An in vitro transamidation assay was performed with PAI-2 immunoprecipitates from *Tbk1*$^{-/-}$ MEFs stably expressing untagged PAI-2 that were left untreated or were stimulated with TNF, and recombinant HA-procaspase-3 generated by in vitro translation was used as a substrate. Caspase-3 cross-linking activity was present in PAI-2 immunoprecipitates but not in control immunoprecipitates, and it was strongly elevated in TNF stimulated cells (Fig. S7*B*). Similarly, TG2 immunoprecipitated from MEFs expressing TG2 and PAI-2 showed inducible transamidation activity toward procaspase-3 (Fig. 4*E*). Assays performed by using recombinant PAI-2 or TG2 further confirmed that the transamidating activity was carried out by TG2 and not by PAI-2 (Fig. 4*E*, *Right*).

We next examined if the protective effect of PAI-2 and TG2 was indeed mediated through inhibition of caspase-3 without affecting alternative (i.e., mitochondrial-mediated) pathways. A slight increase in BID cleavage after stimulation with TNF and CHX was observed in *Tbk1*$^{-/-}$ MEFs relative to WT cells (Fig. S8*A*). Expression of PAI-2 in these cells was unable to prevent BID cleavage (Fig. S8*B*), suggesting that PAI-2 is not a bona fide antiapoptotic factor. We also analyzed TNF-induced apoptosis in cells defective in caspase-3. In agreement with previous studies (28, 29), we found that caspase-3–deficient (*Casp3*$^{-/-}$) MEFs were highly resistant to TNF-induced apoptosis (Fig. S8*C*), highlighting that the absence of caspase-3 does not generate a compensatory cell death pathway (e.g., TNF-induced BID cleavage) in MEFs and that caspase-3 is indeed critical to mediate the TNF response in these cells. Taken together, these experiments clearly indicated that PAI-2 and TG-2 act specifically on TNF-induced, caspase-3–dependent apoptosis.

To examine the antiapoptotic function of TG2, we first used the irreversible TG2 inhibitor KCC009 (30). As shown in Fig. 4*F*, treatment with KCC009 strongly potentiated TNF-induced caspase-3 activation and apoptosis in WT MEFs. To further confirm the antiapoptotic function of TG2, primary MEFs derived from *Tg2*$^{+/+}$ and *Tg2*$^{-/-}$ littermate embryos (31) were examined for their sensitivity to TNF-induced apoptosis. Apoptosis (PARP cleavage) and caspase-3 activation were detected by immunoblotting (Fig. 4*G*). Caspase-3 activation was observed in *Tg2*$^{-/-}$ MEFs treated with TNF without the need for inhibition of de novo protein synthesis, indicating that these cells have an intrinsic defect in the antiapoptotic response to TNF. The extent of cell death was quantified by staining with propidium iodide (PI) (Fig. 4*H*) and FACS analysis after annexin V and PI staining confirmed that *Tg2*$^{-/-}$ MEFs showed increased susceptibility to TNF-induced apoptosis (Fig. S9).

TG2 Is Essential for Prevention of TNF-Dependent Liver Injury. To assess the antiapoptotic function of TG2 in vivo, we used two models of TNF-induced liver injury in mice. WT and *Tg2*$^{-/-}$ mice were first injected intraperitoneally with TNF and actinomycin D (Act D). *Tg2*$^{-/-}$ mice showed clear signs of liver failure such as elevated serum aspartate aminotransferase (AST) and alanine aminotransferase (ALT) levels (Fig. 5*A*), massive infiltration with neutrophils, and presence of numerous apoptotic bodies (Fig. 5*B*). The presence of a high amount of TUNEL-positive cells at the injury sites indicated that cell death mainly occurred through apoptosis (Fig. 5*B*). Caspase-3 activation was also observed in liver extracts from *Tg2*$^{-/-}$ mice injected with TNF and Act D (Fig. 5*C*). To rule out that apoptosis occurred in endothelial cells, staining with anti-CD31 (PECAM-1), which detects endothelial cells, was performed on sections consecutive to those used for histological evaluation and TUNEL assays. The absence of TUNEL-positive cells in the CD31-positive population, combined with histological evaluation, indicated that hepatocytes were the major cell type undergoing apoptosis in TNF/Act D-challenged *Tg2*$^{-/-}$ mice (Fig. 5*B*). *Tg2*$^{+/+}$ mice also experienced liver damage, but the response was much weaker than in *Tg2*$^{-/-}$ mice (Fig. 5*A*) and no caspase-3 activation could be detected (Fig. 5*C*). Thus, *Tg2*$^{-/-}$ mice are more susceptible to TNF-induced liver injury than WT mice. *Tg2*$^{-/-}$ mice were also highly sensitive to T cell-mediated liver injury induced by i.v. injection of Con A, which is TNF-dependent. Liver damage indicated by ALT release was present in both genotypes but was more severe in *Tg2*$^{-/-}$ mice (Fig. 5*D*). Massive hepatocyte cell death detected by TUNEL staining was observed in *Tg2*$^{-/-}$ liver sections 8 h after Con A injection (Fig. 5*E*), and caspase-3 activation indicated that cell death in *Tg2*$^{-/-}$ mice occurred through apoptosis (Fig. 5*F*). Liver destruction was clearly visible 24 h after Con A injection in *Tg2*$^{-/-}$ mice, and the apoptotic cell remnants could no longer be detected by TUNEL reaction. Only few apoptotic hepatocytes were found in liver sections from *Tg2*$^{+/+}$ mice (Fig. 5*E*), and caspase-3 activation was not observed (Fig. 5*F*). These data strongly support the physiological relevance of TG2 as an inhibitor of TNF-induced apoptosis.

Discussion

The role of TBK1 in mediating the innate immune response to viruses and dsDNA through induction of type I IFN is well documented. By contrast, the role of TBK1 in IKK–NF-κB signaling has been debated, because of the observation that, al-

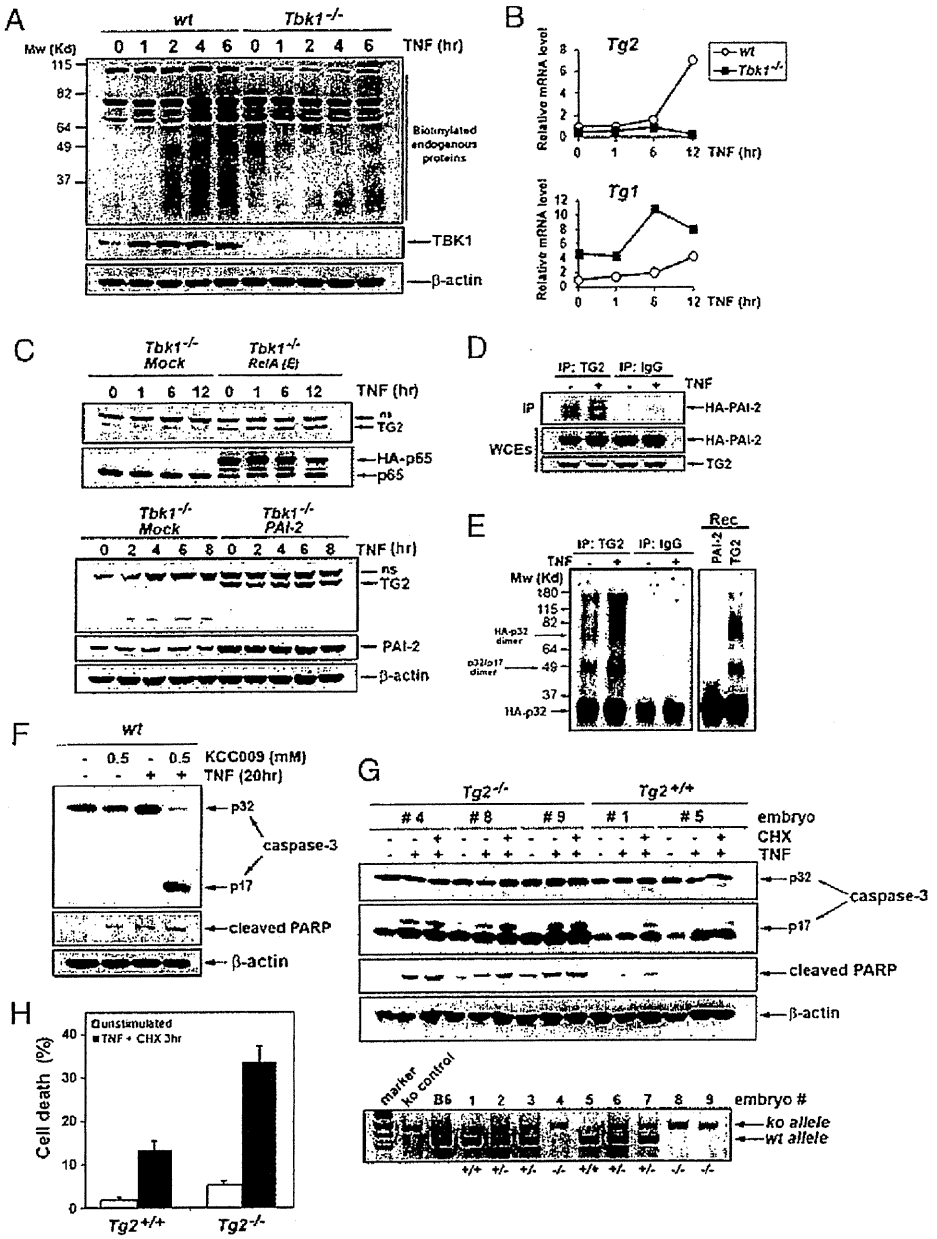

Fig. 4. TG2 is a TBK1-dependent antiapoptotic factor. (*A*) In vivo transamidation activity was determined in WT and *Tbk1*$^{-/-}$ MEFs metabolically labeled with BP and stimulated with TNF for the indicated times. Cell extracts were prepared, and biotin-conjugated proteins were detected by immunoblotting using anti-streptavidin-HRP (Pierce). (*B*) Induction of *Tg* gene expression was determined by qRT-PCR analysis of mRNAs from WT and *Tbk1*$^{-/-}$ MEFs stimulated with TNF for the indicated times. (*C*) Endogenous TG2 protein amounts were determined by immunoblotting in extracts from *Tbk1*$^{-/-}$ MEFs expressing RelA(E) (*Upper*), PAI-2 (*Lower*), or an "empty" retrovirus (mock) and treated with TNF for the indicated times (ns, nonspecific). (*D*) Coimmunoprecipitation of PAI-2 with TG2 was examined in MEFs stably expressing HA-PAI-2 and human TG2 that were left untreated or were stimulated with TNF for 8 h. Control immunoprecipitations were performed with nonimmune IgGs. (*E*) In vitro transamidation assay was performed with TG2 or control immunoprecipitates prepared from untreated or TNF-stimulated *Tbk1*$^{-/-}$ MEFs expressing TG2 and untagged PAI-2 or with recombinant proteins (rec) using HA-procaspase-3 as a substrate. (*F*) Wt MEFs were treated with TNF (20 h) with or without the transglutaminase-specific inhibitor KCC009 (0.5 mM). Caspase-3 activation, PARP cleavage, and protein expression were determined by immunoblotting. (*G*) WT and *Tg2*$^{-/-}$ primary MEFs prepared from littermate embryos were left untreated or treated with TNF alone (20 h) or TNF plus CHX (6 h). Caspase-3 activation and apoptosis were determined as detailed earlier. Genotyping (*Lower*) was performed by PCR amplification as described (31). (*H*) The extent of cell death in WT and *Tg2*$^{-/-}$ MEFs that were stimulated for 3 h with TNF plus CHX was quantified by staining with PI.

though TBK1 affects NF-κB target gene expression, it is not required for activation of NF-κB DNA binding (11). Early studies found TBK1 to form a complex with the adaptor molecules TRAF2 and TANK (8), which mediate assembly of signaling complexes at the intracellular tails of cytokine receptors (32). Indeed, TBK1 is recruited to TNFR1 upon TNF binding (10) and interacts with IKKγ/Nemo, the regulatory subunit of IKK (33, 34). We reported that TBK1 activates NF-κB through phosphorylation-mediated activation of the IKK complex (9). Consistent with a role for TBK1 in NF-κB signaling, *Tbk1*$^{-/-}$

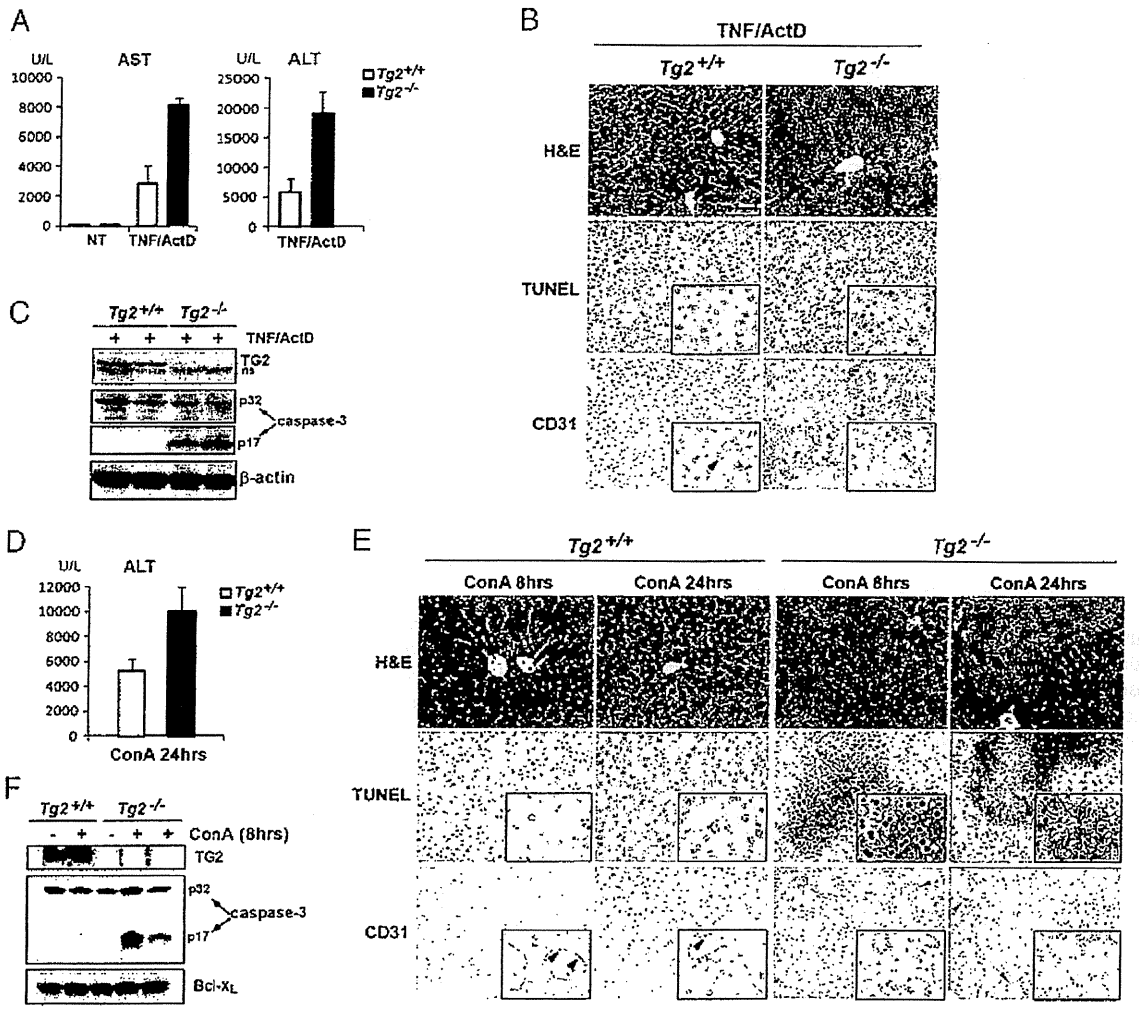

Fig. 5. TG2 protects mice from TNF-dependent liver apoptosis. (*A–C*) WT and $Tg2^{-/-}$ mice were injected with TNF and ActD and analyzed 16 h later. (*A*) Serum AST and ALT levels were determined in untreated mice (NT) or mice treated with TNF and Act D. Data are averages ± SD ($n = 3$). (*B*) Histological analysis (H&E staining), TUNEL staining, and anti-CD31 immunostaining were performed on sequential liver sections of WT and $Tg2^{-/-}$ mice 16 h after TNF and Act D injection. *Insets*: Higher magnification of a selected area. Arrowheads show vascular endothelial cells (CD31-positive), which are TUNEL-negative. CD31 immunostaining in $Tg2^{-/-}$ liver sections displayed some nonspecific background staining as a result of the presence of cell debris. (*C*) Caspase-3 activation was determined by immunoblot analysis of liver protein extracts prepared 16 h after TNF and Act D injection. (*D–F*) The same analyses were performed on WT and $Tg2^{-/-}$ at 8 h (*E* and *F*) or 24 h (*D* and *E*) after injection of Con A (35 mg/kg). (*D*) Serum AST and ALT levels measured after Con A injection. Data are averages ± SD ($n = 2$). (*E*) Histological analysis, TUNEL assays, and anti-CD31 staining were performed on sequential liver sections of WT and $Tg2^{-/-}$ mice at 8 h or 24 h after injection of Con A. *Insets*: Higher magnification of a selected area. TUNEL-positive cells (nuclear staining) in $Tg2^{-/-}$ liver sections are CD31-negative and represent apoptotic hepatocytes. Twenty-four hours of treatment with Con A induced massive liver degeneration in $Tg2^{-/-}$ mice, and dead cells were no longer detectable by TUNEL staining. Arrowheads point to vascular endothelial cells (CD31-positive cells), which are TUNEL-negative. (*F*) Liver extracts prepared from WT and $Tg2^{-/-}$ mice challenged with Con A (8 h) or PBS solution were analyzed for caspase-3 activation.

mice die during embryonic development from massive liver apoptosis and, like $Rela^{-/-}$, $Ikk\beta^{-/-}$, and $Ikk\gamma^{-/-}$ mice, they can be rescued by ablation of TNFR1 (11, 13). Cells derived from $Tbk1^{-/-}$ mice were reported to exhibit normal NF-κB activation without increased sensitivity to TNF-induced apoptosis (11). However, the present results show that TBK1 can directly phosphorylate RelA and thereby control the expression of a subset of NF-κB target genes that inhibit TNF-induced apoptosis. Our findings that $Tbk1^{-/-}$ MEFs are highly susceptible to TNF-induced apoptosis are consistent with the phenotype of $Tbk1^{-/-}$ fetuses, which exhibit all the characteristics of a defective TNF-induced and NF-κB–dependent antiapoptotic response (13). The divergence between our results and those reported earlier may result from different experimental conditions and detection methods. For instance, Bonnard et al. (11), examined cell viability by PI staining after stimulation of MEFs with a low dose of TNF (10 ng/mL), whereas we used a higher dose of TNF (25 ng/mL) without or with CHX and evaluated the apoptotic response by TUNEL assays and direct analysis of caspase-3 cleavage.

Molecular analysis of signaling events downstream of TNFR1 revealed that $Tbk1^{-/-}$ cells exhibit impaired IKK-mediated RelA phosphorylation at Ser^{534}, confirming the earlier suggestion that TBK1 modulates IKK activity (9). Importantly, expression of a phospho-mimic RelA(S534E) variant in $Tbk1^{-/-}$ MEFs restored the antiapoptotic response, demonstrating a specific biological function associated with RelA Ser^{534} phosphorylation, although this phosphorylation event is not critical for activation of most NF-κB target genes. These findings are consistent with previous reports that TNF-induced NF-κB activation is largely

normal in *Tbk1*$^{-/-}$ cells (11). Phosphorylation of RelA at Ser^{534} does not affect most RelA functions, including inhibition by IκBs, nuclear translocation, and binding to target gene promoters (Fig. S3). Instead, it modulates its ability to transactivate a specific subset of NF-κB target genes. Among these, we have identified *Pai-2* as a critical antiapoptotic gene and showed that reexpression of PAI-2 in *Tbk1*$^{-/-}$ MEFs inhibited the TNF-induced apoptotic response. Although NF-κB activation through induced IκB degradation is a well established signaling mechanism, it has long been suspected that expression of individual NF-κB target genes is further modulated through specific posttranslational modifications of NF-κB subunits (35, 36). We now show that one such mechanism involves RelA Ser^{534} phosphorylation, which depends on TBK1 and IKK activity. However, it is not yet clear how TBK1 directs IKK to specifically phosphorylate RelA Ser^{534} while having no effect on other IKK-dependent functions.

We also do not understand what causes the initial activation of caspase-8 in *Tbk1*$^{-/-}$ cells and how PAI-2 affects caspase-8 activation. We showed that cFLIP$_L$ is cleaved in a caspase-dependent manner when *Tbk1*$^{-/-}$ MEFs are stimulated with TNF in the presence of CHX (Fig. S1), and this may prompt initiation of the proapoptotic cascade. This is consistent with previous studies reporting that TNF promotes caspase-8 activation by elimination of cFLIP$_L$ when NF-κB–mediated *cFlip* induction is defective (5), de novo protein synthesis is blocked (37), or cFLIP degradation is enhanced (38). Furthermore, it was recently proposed that, in response to death receptor ligation, cFLIP and caspase-8 could form catalytically inactive heterodimers, which prevent the initiation of apoptosis (39).

Our results suggest that PAI-2 exerts its antiapoptotic function through interaction with and stabilization of TG2, which prevents caspase-3 activation by cross-linking of procaspase-3. Although it remains to be determined whether TG2 can also cross-link other caspases, including caspase-8, this observation provides a missing molecular link that explains the observation made more than a decade ago that the C-D interhelical domain or C-D loop of PAI-2, a conserved protein binding domain among ov-serpin family members (14), was essential for the antiapoptotic function of PAI-2 in TNF-stimulated cells (22). It was postulated that an interaction between the C-D loop and unknown proteins was likely to be important for resistance to apoptosis. We now show that PAI-2 interacts with TG2 in a TNF-dependent manner. This interaction presumably protects TG2 from proteolysis allowing TG2 to cross-link procaspase-3 and promote cell survival. Interestingly, another ubiquitously expressed ov-serpin family member, serpinB10 (PI10), was also found to provide protection against TNF-induced apoptosis (40). The authors observed the formation of high molecular weight SDS-stable PI10-containing complexes in cells treated with TNF in the presence of CHX (40). These complexes were suggested to contain a serine protease that is activated during this process, but this activity was never identified. Nevertheless, these observations raise the hypothesis that some ov-serpins may share a common function in controlling cell death, and that their specific physiological roles may have been obscured as a result of redundancy (14, 41). Although it remains to be further investigated, our observations that PAI-2 and TG2 interact in cells, and mediate a common antiapoptotic response, suggest that these unconventional antiapoptotic factors participate in a posttranslational mechanism that controls caspase-3 activation. Identification of the mechanism that controls TG2 turnover will provide additional insights into this antiapoptotic process.

The tumor suppressor retinoblastoma protein (Rb) is another intracellular target of PAI-2, which protects Rb from cleavage by calpains and thereby contributes to tumor cell survival (42). It was also shown that TG2 could protect Rb from caspase-7–mediated cleavage in fibroblasts (43). In light of our present results, it is tempting to speculate that PAI-2 and TG2 or a related enzyme may also control Rb-dependent cell survival. Notably, PAI-2 was also found to protect macrophages from pathogen-induced cell death (44), acting as a modulator of the innate immune response (45).

The antiapoptotic function of TG2 has been widely debated (25, 46), primarily because no spontaneous cell death was observed in *Tg2*$^{-/-}$ mice (31, 47, 48). However, TG2 protects cancer cells from thapsigargin- or hypoxia-induced death (23, 24), as well as staurosporine-induced apoptosis (49). Initial evidence for the antiapoptotic function of TG2 in vivo came from the work of Sarang et al. (26), who showed that *Tg2*$^{-/-}$ mice were more susceptible to Fas-mediated cell death. We now show in two different models of liver injury triggered by injection of TNF to Act D-sensitized mice or by Con A administration that *Tg2*$^{-/-}$ mice display increased hepatocyte apoptosis relative to WT counterparts (Fig. 5). These data strongly support a role for TG2 in inhibition of cell death mediated by members of the TNF/TNFR1 superfamily. However, an important question that needs to be answered is why *Pai-2*$^{-/-}$ and *Tg2*$^{-/-}$ mice are viable whereas genetic ablation of *Tbk1* leads to embryonic lethality. It could be argued that the newly identified PAI-2 and TG2-dependent pathway is not the only way by which TBK1 inhibits cell death. In addition, PAI-2 may act redundantly with PI10, as mentioned earlier. Furthermore, *Pai-2* is only one of several NF-κB–regulated antiapoptotic genes, such as *cIaps*, *cFlip*, *Bcl-X$_L$*, and others (5, 20), whose expression is needed to suppress TNF-induced liver destruction. Although the antiapoptotic function of these genes has never been disputed, genetic ablation of each one of them in isolation does not result in embryonic lethality as a result of liver failure. The current challenge is to identify the minimal set of antiapoptotic genes that needs to be expressed at a given time and in a particular environmental context during liver development and adult life to suppress TNF-driven hepatocyte death. It will also be interesting to test whether the combined ablation of both *Pai-2* and *Tg2* will result in a more severe phenotype that approaches that of *Tbk1*$^{-/-}$ mice. The identification of additional antiapoptotic factors whose expression or activity depends on TBK1 will shed further light on this question. Such factors may act independently of or in conjunction with the PAI-2–TG2 pathway.

Materials and Methods

Reagents. CHX, puromycin, z-VAD-FMK, MG-132, and protease inhibitors were from Calbiochem, and Act D, Con A, AEBSF, and Polybrene were from Sigma-Aldrich. Recombinant human PAI-2 was from Peprotech. Antibodies against RelA/p65 (S536) (no. 3031), phospho-IκBα (no. 9241), phospho-MAPKs (no. 9910), phospho-cJun (no. 9261), ERK, p38 (no. 9212), TBK1 (no. 3012), Bcl-X$_L$ (no. 2764), c-IAP1 (no. 4952), mBID (no. 2003), caspase-3 (no. 9662), cleaved caspase-3 (no. 9661), and cleaved PARP (no. 9544) were from Cell Signaling; antibodies to IKKγ (no. 557383), JNK1 (no. 551196), XIAP (no. 610716), CD95/Fas receptor (554254), caspase-8 (no. 559932), and procaspase-3 (no. 65906E) were from BD Transduction Laboratories; antibodies to IKKα (no. IMG-136A), IKKβ (no. IMG-129A), TBK1 (IMG-139A), and IκBα (no. IMG-127A) were from Imgenex; antibodies against RelA (sc-372 and sc-372-G), RelB, cRel, IκBβ, HSP60, and PAI-2 (sc-25746) were from Santa Cruz Biotechnology; anti-p65/RelA (CT), anti–phospho-ATF-2 (no. 05–891), anti-TG2 (no. 06–471), and anti-caspase-1 (no. 06–503) were from Upstate Biotechnology; anti–CREB-1 (AB3006) was from Millipore; anti-FLIPα (CT; no. 1161) was from ProSci, anti-TG2 (AB-4) was from Neomarkers (Lab Vision), anti-HA (clone 3F10) was from Roche, anti-cAIP2 was from R&D Systems, and anti-CD31 was from Abcam.

Immunoblotting. Whole-cell extracts were obtained by lysing cells in a buffer containing 50 mM Tris-HCl, pH 7.6, 250 mM NaCl, 1% Triton X-100, 0.5% Nonidet P-40, 3 mM EDTA, 3 mM EGTA, 10% glycerol, 2 mM DTT, 1 mM PMSF, 1 mM sodium orthovanadate, and a protease inhibitor mixture (Calbiochem). Nuclear extracts were prepared using NE-PER Nuclear and Cytoplasmic Extraction Reagents (Pierce). Proteins were separated by SDS/PAGE and blotted onto PVDF membranes (Millipore). The membranes were probed with the

appropriate antibodies and the antigen–antibody complexes detected by SuperSignal Western Pico Luminol/Enhancer solution (Pierce).

Kinase Assays. The IKK complex was immunoprecipitated from cell extracts using an anti-IKKγ antibody and the IKK activity was measured by in vitro kinase assay as described (19, 50) by using GST-IκBα(1-54) or GST-p65(354-551) as substrates.

Phosphorus-32 Metabolic Labeling and Phospho-Peptide Mapping. Cells were labeled with [^{32}P]orthophosphate as previously described (19, 50). Briefly, cells incubated with [^{32}P]orthophosphate (2 mCi/mL) for 5 h were stimulated with TNF (25 ng/mL) for 15 min, washed with PBS solution, and harvested in RIPA buffer. RelA was immunoprecipitated from precleared lysates by using an anti-RelA/p65 antibody (C-20; Santa Cruz Biotechnology). Immune complexes were washed in RIPA buffer. The proteins were resolved by SDS/PAGE and transferred to PVDF membranes (Millipore) for autoradiography and immunoblot analysis. Phospho-peptide mapping of phospho-labeled RelA/p65 was performed as described (19, 50).

Site-Directed Mutagenesis. Site-directed mutagenesis was performed using the Quick Exchange Mutagenesis kit (Stratagene) according to the manufacturer's instructions.

Retroviral Transductions. cDNAs were subcloned into the pLPCX retroviral vector (Stratagene). Recombinant retroviruses were produced by cotransfection with pCL-Eco into Phoenix packaging cells using Lipofectamine Plus reagent (Invitrogen). Supernatants containing recombinant retroviruses were collected 2 d after transfection, filtered to remove cell debris, and used directly for infection. MEFs at subconfluence were infected with viral stocks in the presence of Polybrene at 8 μg/mL, and two or three consecutive infections were performed over a period of 24 h. One day after the last infection, the infected cells were selected in medium supplemented with 2 μg/mL puromycin. Experiments were performed with pools of stable cells.

Gene Silencing Using shRNAs. Retroviral vectors (pRS plasmids) encoding shRNAs specific to mPAI-2 or a scrambled shRNA were purchased from Origene. Production of retroviruses, infection of cells and selection of stable cells were performed as described earlier. The most efficient *Pai-2*–specific shRNA construct among four tested was used.

Apoptosis Assays. Cells gown on Permanox Lab-Tek chamber slides were left untreated or stimulated with TNF (25 ng/mL) in the presence or absence of CHX (10 μg/mL) for the indicated times. Cells were fixed with 4% paraformaldehyde and permeabilized for 5 min with 0.1% Triton X-100 in 0.1% sodium citrate at 4 °C. Apoptotic cells were detected by TUNEL staining (Roche or Promega). DAPI staining was performed for total cell counting.

Immunofluorescence. Cells cultured on Lab-Tek chamber slides were left untreated or stimulated for 30 min with TNF (25 ng/mL). Cells were fixed with 4% paraformaldehyde, and the subcellular localization of RelA/p65 was examined by fluorescent immunostaining by using a polyclonal antibody against p65 (C-20) and Alexa-labeled anti-rabbit purified IgG (Jackson ImmunoResearch).

qRT-PCR and Microarray Analysis. Total RNA was extracted using TRIzol LS (Invitrogen) and purified on RNeasy Miniprep columns (Qiagen). For qRT-PCR analysis, cDNAs were synthesized by using a SuperScript II cDNA synthesis kit (Invitrogen). Real-time PCR amplifications were performed in 96-well optical reaction plates with Power SYBR Green PCR Master Mix (Applied Biosystems). Primers were designed by using Primer Express software. Primer sequences are available upon request. For microarray analysis, preparation of cDNA probes, hybridization to a mouse 10k oligo DNA microarray, scanning of the microarrays, and data analysis were performed by the Nippon Laser and Electronics Lab (Nagoya, Japan).

ChIP Assays. ChIP assays were performed as described (51) by using a polyclonal antibody against RelA/p65 (C-20; Santa Cruz Biotechnology). Samples were analyzed by PCR. Sequence information of the promoter-specific primers is available upon request.

In Vivo Transamidation. Assays were performed essentially as described previously (27). Cells were metabolically labeled with 1 mM pentylamine-biotin (BP; Pierce) added to the culture medium for 1 h before stimulation with TNF (25 ng/mL) for the indicated times. Cells were washed with PBS solution and harvested, and cell extracts were prepared by sonication in urea-containing buffer (50 mM Tris HCl, pH 7.6, 250 mM NaCl, 2 M urea, 0.05% SDS, 40 mM DTT, and a protease inhibitor mixture). Proteins were resolved by SDS/PAGE (10% gel) and transferred onto nitrocellulose membranes (Schleicher and Schuell), and proteins that incorporated BP were detected by using HRP-conjugated streptavidin and chemiluminescence (Pierce).

In Vitro Transamidation Assays. The mouse procaspase-3 cDNA was HA-tagged and subcloned into pBluescript KS(+) (Stratagene). The protein was expressed by in vitro coupled transcription-translation in reticulocyte lysate (Promega), immunoprecipitated with anti-HA beads (Roche), and eluted with HA-peptide. The protein was further incubated with PAI-2 or TG2 immunoprecipitated from cell extracts or with recombinant proteins in a buffer containing 50 mM Tris HCl, pH 8.5, 150 mM NaCl, 5 mM $CaCl_2$, and a protease inhibitor mixture (Calbiochem). The reactions were carried out for 1 h at 37 °C. HA-tagged procaspase-3 was detected by SDS/PAGE and immunoblotting using anti-HA or anti–procaspase-3 antibodies.

Mice. *Tg2*$^{-/-}$ mice were generated by homologous recombination (31) and were back-crossed to C57BL/6 mice for more than eight generations.

Preparation of MEFs. MEFs were prepared from individual littermate embryos at embryonic day 13.5 by using a standard procedure. Briefly, after removal of the head and the liver, the embryonic tissue was washed twice with PBS solution and treated with trypsin/EDTA for 30 min. The homogenates were transferred into a 150-mm dish containing complete culture medium (DMEM supplemented with 10% FBS, 0.1 mM β-mercaptoethanol, and antibiotics). Cells were passaged every 2 to 3 d. Experiments were performed with cells at passages three and four. The genotype of MEFS was determined and confirmed by PCR using genomic DNA extracted from yolk sac and MEFs.

Liver Injury Models. All experimental protocols were conducted in accordance with the Korean law on animal protection and approved by the institutional animal care and use committee at the National Cancer Center of Korea. Mice (9–10 wk old) were injected intraperitoneally with 20 μg of Act D and 0.3 μg of mouse TNF (no.575202; Biolegend). Alternatively, Con A was injected through the tail vein at 35 mg/kg. In both cases, PBS solution was injected in control animals. Mice were killed 8 h, 24 h (Con A), or 16 h (TNF and Act D) after challenge. Blood was collected by cardiac puncture, and the livers were surgically removed. Serum ALT and AST levels were determined by using Fuji Dri-Chem Slides AST-/ALT-PIII (FujiFilm) according to the manufacturer's instructions. Liver tissue samples were fixed in 10% buffered formalin and processed for paraffin embedding and histological evaluation. Pieces of liver tissue were snap-frozen and used for preparation of whole-liver protein extracts. Histological analysis was performed on liver sections (2–3 μm thick) after routine H&E staining. In situ TUNEL assays were performed on tissue sections by using an in situ apoptosis detection kit (Takara Bio) according to the manufacturer's instructions. Briefly, deparaffinized sections were treated with proteinase K and washed with PBS solution, and endogenous peroxidase activity was inactivated in 3% H_2O_2. After terminal-deoxynucleotidyl transferase enzymatic reaction, the signal was detected by using an HRP-labeled anti-FITC antibody and visualized with DAB as substrate.

Immunohistochemistry. Deparaffinized tissue sections were incubated with anti-CD31 (PECAM-1; Abcam) at a dilution of 1:50. Antibody binding was detected by using a HRP-linked secondary antibody and revealed by conventional immunostaining performed in an autoimmunostaining apparatus (HX System; Ventana) using DAB as substrate.

ACKNOWLEDGMENTS. We thank D. Rothwarf for critical reading of the manuscript and helpful suggestions; W.-C. Yeh, S. Akira, A. Beg, A. Hoffmann, R. Flavell, and Z.-W. Li for providing *Tbk1*$^{-/-}$, *RelA/p65*$^{-/-}$, *IκBα*$^{-/-}$, *caspase-3*$^{-/-}$, and *Ikkαlβ*$^{-/-}$ MEFs, respectively; P. Brouckaert for providing mTNF; M. Hernandez (Applied Biosystems) for advice on quantitative PCR; C. H. Jeon for technical assistance; and D. Ginsburg, M. Montminy, T. Kato, and S. Imajoh-Ohmi for plasmids and antibodies. M.D. was supported by a grant from the Claudia Adams Barr Program in Cancer Research. K.S.K. was supported by the National Institutes of Health (NIH). This work was supported by National Cancer Center (Korea) Research Grants NCC 0510270 and NCC1110011-1 (to H.L. and S-Y.K.), National Research Foundation Grant 2010-0029919 funded by the Korean government (to S-Y.K.), NIH Grant AI043477 (to M.K.), and Grants-in-Aid for Scientific Research on Priority Area and for Scientific Research (B) by the Ministry of Education, Science, Sports, and Culture of Japan (M.N.), M.K. is an American Cancer Society Research Professor.

1. Green DR, Evan GI (2002) A matter of life and death. *Cancer Cell* 1:19–30.
2. Li J, Yuan J (2008) Caspases in apoptosis and beyond. *Oncogene* 27:6194–6206.
3. Chen G, Goeddel DV (2002) TNF-R1 signaling: A beautiful pathway. *Science* 296: 1634–1635.
4. Wajant H, Scheurich P (2011) TNFR1-induced activation of the classical NF-κB pathway. *FEBS J* 278:862–876.
5. Karin M, Lin A (2002) NF-kappaB at the crossroads of life and death. *Nat Immunol* 3: 221–227.
6. Burstein E, Duckett CS (2003) Dying for NF-kappaB? Control of cell death by transcriptional regulation of the apoptotic machinery. *Curr Opin Cell Biol* 15:732–737.
7. Janes KA, et al. (2006) The response of human epithelial cells to TNF involves an inducible autocrine cascade. *Cell* 124:1225–1239.
8. Pomerantz JL, Baltimore D (1999) NF-kappaB activation by a signaling complex containing TRAF2, TANK and TBK1, a novel IKK-related kinase. *EMBO J* 18:6694–6704.
9. Tojima Y, et al. (2000) NAK is an IkappaB kinase-activating kinase. *Nature* 404: 778–782.
10. Kuai J, et al. (2004) NAK is recruited to the TNFR1 complex in a TNFalpha-dependent manner and mediates the production of RANTES: identification of endogenous TNFR-interacting proteins by a proteomic approach. *J Biol Chem* 279:53266–53271.
11. Bonnard M, et al. (2000) Deficiency of T2K leads to apoptotic liver degeneration and impaired NF-kappaB-dependent gene transcription. *EMBO J* 19:4976–4985.
12. Hemmi H, et al. (2004) The roles of two IkappaB kinase-related kinases in lipopolysaccharide and double stranded RNA signaling and viral infection. *J Exp Med* 199:1641–1650.
13. Gerondakis S, et al. (2006) Unravelling the complexities of the NF-kappaB signalling pathway using mouse knockout and transgenic models. *Oncogene* 25:6781–6799.
14. Izuhara K, Ohta S, Kanaji S, Shiraishi H, Arima K (2008) Recent progress in understanding the diversity of the human ov-serpin/clade B serpin family. *Cell Mol Life Sci* 65:2541–2553.
15. Liu ZG, Hsu H, Goeddel DV, Karin M (1996) Dissection of TNF receptor 1 effector functions: JNK activation is not linked to apoptosis while NF-kappaB activation prevents cell death. *Cell* 87:565–576.
16. Tang G, et al. (2001) Inhibition of JNK activation through NF-kappaB target genes. *Nature* 414:313–317.
17. Fujita F, et al. (2003) Identification of NAP1, a regulatory subunit of IkappaB kinase-related kinases that potentiates NF-kappaB signaling. *Mol Cell Biol* 23:7780–7793.
18. Buss H, et al. (2004) Constitutive and interleukin-1-inducible phosphorylation of p65 NF-kappaB at serine 536 is mediated by multiple protein kinases including IkappaB kinase (IKK)-alpha, IKKbeta, IKKepsilon, TRAF family member-associated (TANK)-binding kinase 1 (TBK1), and an unknown kinase and couples p65 to TATA-binding protein-associated factor II31-mediated interleukin-8 transcription. *J Biol Chem* 279: 55633–55643.
19. Delhase M, Hayakawa M, Chen Y, Karin M (1999) Positive and negative regulation of IkappaB kinase activity through IKKbeta subunit phosphorylation. *Science* 284: 309–313.
20. Pahl HL (1999) Activators and target genes of Rel/NF-kappaB transcription factors. *Oncogene* 18:6853–6866.
21. Kumar S, Baglioni C (1991) Protection from tumor necrosis factor-mediated cytolysis by overexpression of plasminogen activator inhibitor type-2. *J Biol Chem* 266: 20960–20964.
22. Dickinson JL, Norris BJ, Jensen PH, Antalis TM (1998) The C-D interhelical domain of the serpin plasminogen activator inhibitor-type 2 is required for protection from TNF-alpha induced apoptosis. *Cell Death Differ* 5:163–171.
23. Yamaguchi H, Wang HG (2006) Tissue transglutaminase serves as an inhibitor of apoptosis by cross-linking caspase 3 in thapsigargin-treated cells. *Mol Cell Biol* 26: 569–579.
24. Jang GY, et al. (2010) Transglutaminase 2 suppresses apoptosis by modulating caspase 3 and NF-kappaB activity in hypoxic tumor cells. *Oncogene* 29:356–367.
25. Lorand L, Graham RM (2003) Transglutaminases: Crosslinking enzymes with pleiotropic functions. *Nat Rev Mol Cell Biol* 4:140–156.
26. Sarang Z, et al. (2005) Tissue transglutaminase (TG2) acting as G protein protects hepatocytes against Fas-mediated cell death in mice. *Hepatology* 42:578–587.
27. Shin DM, et al. (2004) Cell type-specific activation of intracellular transglutaminase 2 by oxidative stress or ultraviolet irradiation: implications of transglutaminase 2 in age-related cataractogenesis. *J Biol Chem* 279:15032–15039.
28. Lakhani SA, et al. (2006) Caspases 3 and 7: Key mediators of mitochondrial events of apoptosis. *Science* 311:847–851.
29. Masud A, et al. (2007) Endoplasmic reticulum stress-induced death of mouse embryonic fibroblasts requires the intrinsic pathway of apoptosis. *J Biol Chem* 282: 14132–14139.
30. Siegel M, Khosla C (2007) Transglutaminase 2 inhibitors and their therapeutic role in disease states. *Pharmacol Ther* 115:232–245.
31. Kim DS, et al. (2010) Transglutaminase 2 gene ablation protects against renal ischemic injury by blocking constant NF-κB activation. *Biochem Biophys Res Commun* 403: 479–484.
32. Napolitano G, Karin M (2010) Sphingolipids: The oil on the TRAFire that promotes inflammation. *Sci Signal* 3:pe34.
33. Chariot A, et al. (2002) Association of the adaptor TANK with the I kappa B kinase (IKK) regulator NEMO connects IKK complexes with IKK epsilon and TBK1 kinases. *J Biol Chem* 277:37029–37036.
34. Bouwmeester T, et al. (2004) A physical and functional map of the human TNF-alpha/NF-kappa B signal transduction pathway. *Nat Cell Biol* 6:97–105.
35. Ghosh S, Karin M (2002) Missing pieces in the NF-kappaB puzzle. *Cell* 109(suppl): S81–S96.
36. Perkins ND (2006) Post-translational modifications regulating the activity and function of the nuclear factor kappa B pathway. *Oncogene* 25:6717–6730.
37. Wang L, Du F, Wang X (2008) TNF-alpha induces two distinct caspase-8 activation pathways. *Cell* 133:693–703.
38. Chang L, et al. (2006) The E3 ubiquitin ligase itch couples JNK activation to TNFalpha-induced cell death by inducing c-FLIP(L) turnover. *Cell* 124:601–613.
39. Green DR, Oberst A, Dillon CP, Weinlich R, Salvesen GS (2011) RIPK-dependent necrosis and its regulation by caspases: A mystery in five acts. *Mol Cell* 44:9–16.
40. Schleef RR, Chuang TL (2000) Protease inhibitor 10 inhibits tumor necrosis factor alpha -induced cell death. Evidence for the formation of intracellular high M(r) protease inhibitor 10-containing complexes. *J Biol Chem* 275:26385–26389.
41. Dougherty KM, et al. (1999) The plasminogen activator inhibitor-2 gene is not required for normal murine development or survival. *Proc Natl Acad Sci USA* 96: 686–691.
42. Tonnetti L, et al. (2008) SerpinB2 protection of retinoblastoma protein from calpain enhances tumor cell survival. *Cancer Res* 68:5648–5657.
43. Boehm JE, Singh U, Combs C, Antonyak MA, Cerione RA (2002) Tissue transglutaminase protects against apoptosis by modifying the tumor suppressor protein p110 Rb. *J Biol Chem* 277:20127–20130.
44. Park JM, et al. (2005) Signaling pathways and genes that inhibit pathogen-induced macrophage apoptosis—CREB and NF-kappaB as key regulators. *Immunity* 23: 319–329.
45. Medcalf RL (2011) Plasminogen activator inhibitor type 2: Still an enigmatic serpin but a model for gene regulation. *Methods Enzymol* 499:105–134.
46. Fesus L, Piacentini M (2002) Transglutaminase 2: An enigmatic enzyme with diverse functions. *Trends Biochem Sci* 27:534–539.
47. De Laurenzi V, Melino G (2001) Gene disruption of tissue transglutaminase. *Mol Cell Biol* 21:148–155.
48. Nanda N, et al. (2001) Targeted inactivation of Gh/tissue transglutaminase II. *J Biol Chem* 276:20673–20678.
49. Rossin F, D'Eletto M, Macdonald D, Farrace MG, Piacentini M (2011) TG2 transamidating activity acts as a reostat controlling the interplay between apoptosis and autophagy. *Amino Acids*, 10.1007/s00726-011-0899-x.
50. Delhase M (2003) IkappaB kinase and NF-kappaB signaling in response to pro-inflammatory cytokines. *Methods Mol Biol* 225:7–17.
51. Saccani S, Pantano S, Natoli G (2002) p38-Dependent marking of inflammatory genes for increased NF-kappa B recruitment. *Nat Immunol* 3:69–75.

OPEN ACCESS Freely available online PLoS one

Genetic Variation of the IL-28B Promoter Affecting Gene Expression

Masaya Sugiyama[1,2,5], Yasuhito Tanaka[3], Takaji Wakita[4], Makoto Nakanishi[2], Masashi Mizokami[1]*

1 The Research Center for Hepatitis and Immunology, National Center for Global Health and Medicine, Ichikawa, Chiba, Japan, 2 Department of Biochemistry and Cell Biology, Nagoya City University Graduate School of Medical Sciences, Mizuho, Nagoya, Japan, 3 Department of Virology and Liver Unit, Nagoya City University Graduate School of Medical Sciences, Mizuho, Nagoya, Japan, 4 Department of Virology II, National Institute of Infectious Diseases, Shinjuku, Tokyo, Japan, 5 JSPS Research Fellow, Japan Society for the Promotion of Science, Chiyoda, Tokyo, Japan

Abstract

The current standard of care for the treatment of chronic hepatitis C is pegylated interferon-α (PEG-IFNα) and ribavirin (RBV). The treatment achieves a sustained viral clearance in only approximately 50% of patients. Recent whole genome association studies revealed that single nucleotide polymorphisms (SNPs) around *IL-28B* have been associated with response to the standard therapy and could predict treatment responses at approximately 80%. However, it is not clear which SNP is most informative because the genomic region containing significant SNPs shows strong linkage disequilibrium. We focused on SNPs in close proximity to the *IL-28B* gene to evaluate the function of each and identify the SNP affecting the *IL-28B* expression level most. The structures of *IL-28A/B* from 5′ to 3′-UTR were determined by complete cDNA cloning. Both *IL-28A* and *28B* genes consisted of 6 exons, differing from the CCDS data of NCBI. Two intron SNPs and a nonsynonymous SNP did not affect *IL-28B* gene function and expression levels but a SNP located in the proximal promoter region influenced gene expression. A (TA) dinucleotide repeat, rs72258881, located in the promoter region was discovered by our functional studies of the proximal SNPs upstream of *IL-28B*; the transcriptional activity of the promoter increased gradually in a (TA)$_n$ length-dependent manner following IFN-α and lipopolysaccharide stimulation. Healthy Japanese donors exhibited a broad range of (TA) dinucleotide repeat numbers from 10 to 18 and the most prevalent genotype was 12/12 (75%), differing from the database (13/13). However, genetic variation of *IL-28A* corresponding to that of *IL-28B* was not detected in these Japanese donors. These findings suggest that the dinucleotide repeat could be associated with the transcriptional activity of *IL-28B* as well as being a marker to improve the prediction of the response to interferon-based hepatitis C virus treatment.

Citation: Sugiyama M, Tanaka Y, Wakita T, Nakanishi M, Mizokami M (2011) Genetic Variation of the *IL-28B* Promoter Affecting Gene Expression. PLoS ONE 6(10): e26620. doi:10.1371/journal.pone.0026620

Editor: John E. Tavis, Saint Louis University, United States of America

Received June 29, 2011; **Accepted** September 29, 2011; **Published** October 25, 2011

Funding: This work was supported by a Grant-in-Aid from the Ministry of Health Labor and Welfare of Japan and a Grant-in-Aid from the Ministry of Education, Culture, Sports, Science, and Technology of Japan (271000) and The Grant of National Center for Global Health and Medicine (22–302). The funders had no role in study design, data collection and analysis, decision to publish, or preparation of the manuscript.

Competing Interests: The authors have declared that no competing interests exist.

* E-mail: mmizokami@hospk.ncgm.go.jp

Introduction

A novel group of cytokines was discovered simultaneously by two independent groups in 2003 and named interferon lambda (IFN-λ) [1,2] or type III IFN. Type III IFN comprises three members, IFN-λ1, 2, and 3 or *IL-29* and *IL-28A*, and *IL-28B*, respectively. Type III IFN is a member of the class II cytokine family. This family includes type I, II, and III interferons and the IL-10 family (IL-10, IL-19, IL20, IL-22, IL-24, and IL-26). IFN-λ uses a distinct receptor complex consisting of a unique subunit, named IFN-λR1, and the IL-10R2 subunit. Expression of the IFN-λR1 receptor subunit is highly restricted, whereas the type I IFN receptor complex and the IL-10R2 receptor were detected in most cell types [1,2,3,4,5,5]. The IL-10R2 receptor subunit is shared by IL-10, IL-22, IL-24, IL-26, and IFN-λ. This suggests that type III IFNs act in a rather cell-type specific manner to mediate their biological functions. Type III IFNs trigger a type I IFN-like gene expression profile [5,6,7], which has been shown to have antiviral activity *in vitro* and *in vivo* [1,2,5,6,8]. Thus, the two types of IFN seem to have similar biological effects at a cellular level. IFN-α and IL-29/28A treatment reduced the concentration of hepatitis C virus (HCV) plus-strand RNA in an *in vitro* assay [6,9,10,11]. In addition, IL-29 may have therapeutic value against chronic viral hepatitis in human patients [5].

Recently, a genome-wide association study (GWAS) revealed that several highly correlated common single nucleotide polymorphisms (SNPs), in a linkage disequilibrium (LD) block encompassing the *IL-28B* genes on chromosome 19q13, are implicated in the response of chronic hepatitis C (CHC) patients to pegylated IFN-alpha (PEG-IFNα) and ribavirin (RBV) [12,13,14]. The CC genotype of rs12979860 and TT genotype of rs8099917 are associated in CHC patients with a sustained viral response (SVR) of 2.5 or greater rate, which is dependent of ethnicity, compared to the other genotypes. Moreover, the CC genotype of rs12979860 and TT genotype of rs8099917 favor spontaneous clearance of HCV [15].

We have reported the genomic analysis of approximately 15 kb containing the significant SNPs using Haploview software for LD and haplotype structure [14,16]. To analyze the difference in LD pattern between races, we performed LD mapping with these SNPs on JPT (Japanese in Tokyo), CEU (Utah residents with ancestry from Northern and Western Europe) or YRI (Yoruba in

Ibada, Nigeria) populations. These SNPs were in strong LD in JPT and CEU populations, although relatively low LD was predicted in the YRI population [14,16], suggesting that any of the SNPs located in this region could be responsible for treatment response. Because of the strong LD, tests for independence among these variants were not able to reveal which of these SNPs is uniquely responsible for the association with virological response (VR) or non-virological response (NVR). The identification of the primary genetic variant located in the LD block remained critical, although the risk haplotype tended to influence the expression levels or activity of *IL-28B* [13,14]. In this study, we sought to determine the primary SNP affecting IL-28B expression and/or its function by focusing on the proximal regulatory region of *IL-28B*.

IL-28B was discovered as a member of the IFN-λ family by Sheppard et al. and Kotenko et al. [1,2]. They discovered this family, *IL-29*, *IL-28A*, and *IL-28B* and the specific receptor, *IL-28RI*, by applying individual computational techniques to the draft human genome. However, the start codon of IFN-λ differs between the reports, with an additional 12 nucleotides at the N-terminus in all IFN-λs reported by Sheppard et al. (Fig. S1). The sequence similarity between these ORFs is approximately 96.7% and, especially, there is a high degree of identity between *IL-28A* and *IL-28B* cDNA (approximately 98%). Figure 1A shows the locations of *IL-28A/B* gene, the significant SNPs around *IL-28B* related to anti-HCV therapy reported in previous studies [12,13,14], and $(TA)_n$ repeats in the regulatory region of *IL-28A* and *B*. The SNPs information assessed in this study is summarized in Table 1 and the locations of the SNPs are shown in the schematic of the *IL-28B* gene (Fig. 1B). The reference sequences of *IL-28A* or *IL-28B* cDNA, registered in NCBI CCDS, are composed of 6 exons and 5 exons, respectively (Fig. 1B). Because high sequence similarity was observed between *IL-28A* and *IL-28B* from CpG to the region downstream of 3'-UTR (Fig. S2), the genes were almost completely identical around transcription start site (TSS) (>99%). Then, we determined the likely gene structure using a complete cDNA cloning method because a similar transcriptional mechanism was expected for *IL-28A* and *IL-28B*.

Materials and Methods

Genome samples

Genome samples were obtained from 20 healthy volunteers (HV). Peripheral blood mononuclear cells (PBMC) collected from HV were isolated using the BD Vacutainer CPT Method (BD Biosciences). Genomic DNAs were extracted by standard methods. SNPs were selected from the database at GWAS database (https://gwas.lifesciencedb.jp/cgi-bin/gwasdb/gwas_top.cgi). Written informed consent was provided by all participants in the genotyping study following procedures approved by the Ethical Committee at Nagoya City University.

Cell lines

Human hepatocellular carcinoma cell lines, HepG2 and HuH7, human hepatocyte cell lines, HuSE2 (kindly provided by Dr. Hijikata in Kyoto University), and the human cervical cancer cell line, HeLa (obtained from The American Type Culture Collection), were cultured in Dulbecco's modified Eagle's medium supplemented with 10% (v/v) fetal bovine serum, 100 U ml^{-1} penicillin and 100 mg ml^{-1} streptomycin. Human leukemia virus type 1 transformed cell line, MT-2 (a gift from Dr. Ueda in Nagoya City University), Burkitt lymphoma cell line, Raji, and human T cell leukemia cell line, Jurkat (obtained from The American Type Culture Collection), were cultured in RPMI 1640 medium supplemented with 10% (v/v) fetal bovine serum, 100 U ml^{-1} penicillin and 100 mg ml^{-1} streptomycin. All incubations were performed at 37°C in a 5% CO_2 gassed incubator. Recombinant human IFN-λ2 and -3 were purchased from R&D Systems (Abingdon, UK). Natural human IFN-α was

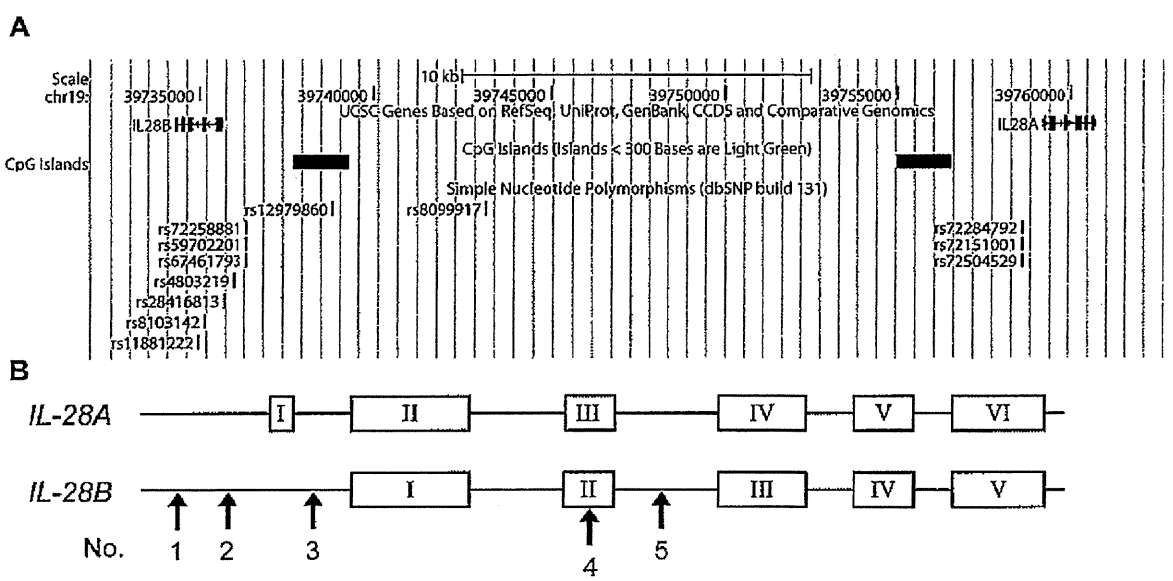

Figure 1. The position of significant SNPs and IL-28A/B in chromosome 19, retrieved from the database. (A) The *IL-28A/B* genes located in chromosome 19q13 are described in the genome map of the UCSC genome browser. The significant proximal SNPs around *IL-28B* associated with response to PEG-IFN/RBV therapy are shown in the map [14]. SNPs of $(TA)_n$ variation at the regulatory region of *IL-28A* are displayed in the position corresponding to that of *IL-28B*, which is not associated with anti-HCV therapy. (B) The schematic of *IL-28A/B* gene structure is described based NCBI CCDS data. Arrows show five significant SNPs examined in this study (see Table 1).
doi:10.1371/journal.pone.0026620.g001

Table 1. Significant SNPs around *IL-28B*.

Feature	rs ID	Allele 1/2*[1]	Minus strand*[2]	Location	No.
DIP*[3]	rs72258881*[4]	ATAT/-	TATA/-	Regulatory	
Substitution	rs4803219	C/T	G/A	Regulatory	2
	rs28416813	C/G	G/C	Intron	3
	rs8103142	T/C	A/G	Nonsynonymous	4
	rs11881222	A/G	T/C	Intron	5

*[1]These data were derived from dbSNP. Allele 2 is the risk allele of HCV therapy reported by Tanaka *et al.*, except for rs72258881.
*[2]Complementary nucleotides are shown because *IL-28B* is coded on the minus strand.
*[3]DIP: deletion/insertion polymorphism.
*[4]The ID represents rs72258881, rs59702201, and rs67461793 because these three are located in the same genomic region, the TA repeat.
doi:10.1371/journal.pone.0026620.t001

purchased from Hayashibara co. ltd. (Okayama, Japan). The mRNA expression levels of receptors stimulated in this study were confirmed by PCR using gene specific primer (Table S1 and Fig. S3),

Plasmid Construction

As a T/G heterozygote genome of rs8099917 with a strong LD was used as the PCR template, amplicons from the major and minor alleles were obtained for the assay described below. PCR was carried out to amplify the fragment from −858 nt of the ATG site to TGA of *IL-28B*, and the products were inserted into pcDNA3.1/Hyg (pcDNA/MA or mi) or pcDNA3.1/Hyg vector deleting CMV promoter (pdCMV/MA or mi). A FLAG sequence was conjugated to 6th exon, removing the stop codon, for real time PCR analysis. The promoter region from nucleotide position −858 to +30 of *IL-28B* was amplified using pdCMV/MA or mi vector and inserted into pGL4 vector for the luciferase assay. A vector with an antisense insert was prepared as a control. For expression constructs, the wild type (WT) plasmids, pcDNA3.1/wild expressing human IL-28B, and pcDNA3.1/ns-mut expressing human IL-28B harboring a K^{74}R mutation, were generated using pcDNA3.1/V5-His-TOPO® (Invitrogen, San Diego, CA) and were used in the subsequent transfections. In addition, pcDNA3.1/AS expressing antisense strand of IL-28B was constructed as a control. We also obtained a pISRE-luc plasmid (provided by Sakamoto N., Tokyo Medical Dental University, Tokyo, Japan). The pGL4.74 vector encoding Renilla Luciferase was purchased from Promega (Madison, WI). These primer sequences are available on request. The above expression vectors were modified for the analysis of splicing function by introducing two intron SNPs (rs28416813 and rs11881222) (Table 1), which were pcDNA/WT, d-iSNPs.

Transient transfections

Transient transfections of HeLa, Jurkat, Raji, HuH7, HepG2, or HuSE2 (hepatocellular carcinomas cell line) cells were carried out using FuGene HD (Roche) or the Cell Line Nucleofector kit (Amaxa Biosystems) according to the manufacturers' protocols. Briefly, Cells (2×10^5) were seeded into a 6 well plate and transfected with for FuGene HD. For the electroporation method, cells (1.0×10^6) were collected and resuspended in Nucleofector solution V for each individual transfection sample.

5′-, 3′-RACE based on full-length cDNA cloning

Total RNA was prepared from cell lines stimulated with lipopolysaccharide (LPS) (0127:B8, Sigma-Aldrich) for 4 hours after 100 U/mL of IFN-α for 16 hours by following previous paper [17]. A GeneRacer Kit (Invitrogen Life Technologies) was used to obtain the complete cDNA sequence of *IL-28A/B* following manufacturer's instructions. Briefly, the GeneRacer RNA Oligo was ligated to the 5′ end specifically of full-length mRNA within the total RNA mixture. This ligated mRNA was then converted to cDNA using reverse transcriptase (RT) and the GeneRacer Oligo dT Primer. Next, this cDNA was used for PCR using the oligonucleotides of GeneRacer 5′ Primer and P1 primer which hybridized to the coding strand of the *IL28A/B* (Table S1). The resulting PCR products were then used for a second round of PCR using the oligonucleotides GeneRacer 5′ Nested Primer, which represents the DNA equivalent of the 3′ end of the GeneRacer RNA Oligo, and P2, which hybridizes to the coding strand of the *IL-28A/B* 5′ to the P1 hybridization site. For 3′ RACE, the cDNA was subjected to the polymerase chain reaction (PCR) to amplify the 3′ end using a forward gene-specific primer P3 designed from *IL-28A/B* and the GeneRacer 3′ primer provided with the kit. Nested PCR, using the same gene-specific primer and GeneRacer 3′ nested primer, was performed. The PCR product of 5′ and 3′ RACE was cloned into pCR4-TOPO TA vector according to the manufacturer's instructions (Invitrogen). Ten clones were isolated and subjected to automated sequencing (ABI3100, ABI) in our core facility.

Protein expression and purification

Recombinant IL-28B and its mutant were produced by transfecting Free-Style™ 293-F cells (purchased from Invitrogen, Carlsbad, CA) with the expression plasmid, which was grown in 5000 ml of FreeStyle 293 Expression Medium, following the manufacturer's recommendations (Invitrogen, Carlsbad, CA). Cultures were maintained at >90% viability on a shaker plate (Titer Plate Shaker; Lab-Line Instruments, Melrose Park, NJ) moving at 125 rpm in a 37°C incubator with 8% CO_2 and subculturing at a 1:10 ratio upon reaching a density of 2×10^6 cells per ml. Cell density and viability were evaluated with a hemocytometer using 0.4% trypan blue staining. After 96 h, the transfected cell culture was harvested. The supernatant containing the secreted recombinant protein was centrifuged (100×g, 15 min), frozen, and stored at −30°C until use. The 293-F cells supernatant containing the recombinant protein was loaded onto a Ni^{2+} column (Amersham Biosciences) following the manufacturer's directions. Fractions were eluted with 80, 100, 250, and 1000 mM imidazole (in 50 mM Tris, 300 mM NaCl, pH 8.0), and the fraction eluted at 250 mM was pooled and concentrated in an Amicon (10 kDa molecular weight cutoff) to 1 ml (Amersham Biosciences).

Western blot analyses

Purified recombinant protein was loaded onto 12% sodium dodecyl sulfate gels. Proteins were detected with goat anti-IL28 (1:2000) polyclonal antibody (Santa Cruz Biotechnology, Santa Cruz, CA) and the secondary antibody. Proteins were visualized using ECL Plus Western blotting detection reagents (GE Healthcare) and a LuminoImager (LAS-3000; Fujifilm). The band densities were analyzed with the Multi Gauge software (version 3.1; Fujifilm).

IL-28A/B promoter genotyping

Germ-line DNA was extracted from PBMC according to standard methods [14]. Twenty HV samples were genotyped for the dinucleotide insertion/deletion (indel) present in the promoter region of *IL-28A* or *B*, as described below. Twenty ng of genomic DNA were subjected to PCR analysis in 50 µl aliquots containing

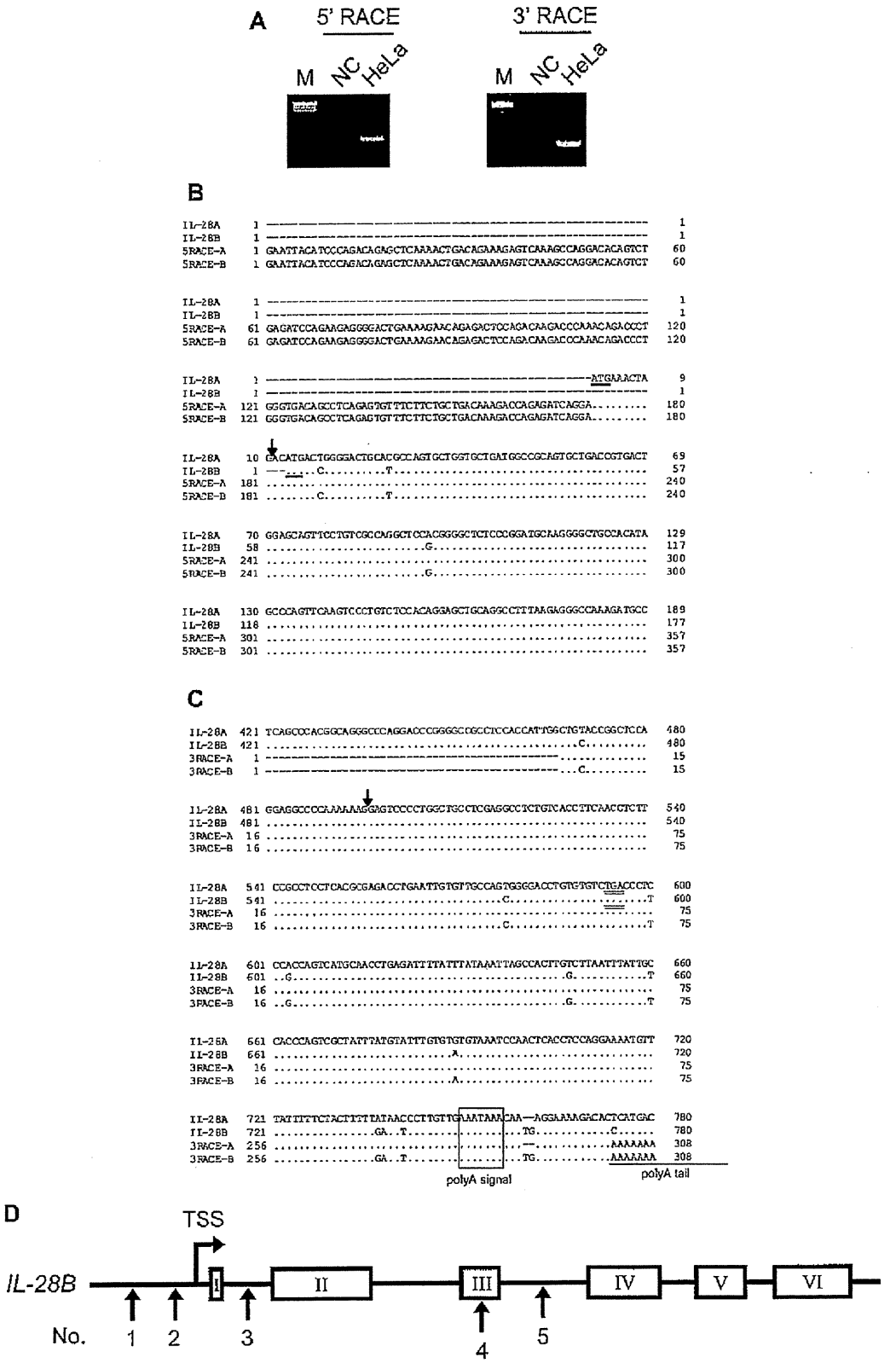
A
5' RACE
3' RACE
M
NC
HeLa
M
NC
HeLa
B
C
polyA signal
polyA tail
D
TSS
IL-28B
I
II
III
IV
V
VI
No.
1
2
3
4
5